A new strategy toward synthesis of novel bifunctional N- and S-bearing sorbent for platinum(IV) removal from aqueous solutions and acidic leaching residue of Pt/Al2O3 catalyst

Mohammed Hamza, Guibal Eric, Yuezhou Wei, Shunyan Ning, Xiangbiao Yin, Amr Fouda, Hamada Amer, Saly El Dakkony

Sustainable Materials and Technologies 42 (2024) e01165

Contents lists available at ScienceDirect

Sustainable Materials and Technologies

journal homepage: www.elsevier.com/locate/susmat

A new strategy toward synthesis of novel bifunctional N- and S-bearing sorbent for platinum(IV) removal from aqueous solutions and acidic leaching residue of Pt/Al_2O_3 catalyst

Mohammed F. Hamza [a,b], Eric Guibal [c,*], Yuezhou Wei [a,d], Shunyan Ning [a], Xiangbiao Yin [a,*], Amr Fouda [e], Hamada H. Amer [f], Saly R. El Dakkony [g]

[a] School of Nuclear Science and Technology, University of South China, Heng Yang 421001, China
[b] Nuclear Materials Authority, POB 530, El-Maadi, Cairo, Egypt
[c] Polymers Composites and Hybrids (PCH), IMT Mines Ales, Ales, France
[d] School of Nuclear Science and Engineering, Shanghai Jiao Tong University, Shanghai, China
[e] Botany and Microbiology Department, Faculty of Science, Al-Azhar University, Nasr City, Cairo 11884, Egypt
[f] Department of Chemistry, Turabah University College, Taif University, Turabah, Saudi Arabia
[g] Egyptian Mineral Resources Authority, Cairo, Egypt

ARTICLE INFO

Keywords:
N- and S-bearing sorbent
Platinum ion-exchange and chelation
Sorption isotherms and uptake kinetics
Metal desorption and sorbent recycling
Sorption selectivity for chloroanions and soft metals

ABSTRACT

Strong incentive politics have been elaborated for promoting the recovery of precious metals from secondary resources. Solid leaching generates acidic effluents that can be pre-treated using precipitation steps for partial separation before applying sorption for metal recovery from mild acidic solutions. For this purpose, a new sorbent was designed carrying numerous N- and S-bearing reactive groups with good affinity for platinum (as chloroanionic species). Thiazole precursors were first reacted before being grafted (by free radical reaction) with triallyl cyanurate (to form CTTR sorbent). The material was characterized by a series of analytical tools (SEM, BET, FTIR, XPS, TGA, elemental analysis, and titration). The effect of pH combined with FTIR and XPS spectroscopy analyses allowed identifying the mechanisms involved in metal binding: electrostatic attraction of chloroplatinate anions with protonated amine groups (especially in acidic conditions), while at moderate acidic pH, metal sorption proceeds through ligand exchange and chelation onto N-based and S-based groups. Optimum sorption was found at pH close to 4 (near pH_{pzc} value). Under selected experimental conditions, the equilibrium was reached in 25–35 min. The pseudo-first order rate equation fitted well experimental profile (though the resistance to intraparticle diffusion contributed to the kinetic control). The maximum sorption capacity at room temperature reached up to 1.58 mmol Pt g^{-1} (at pH 4). The sorption isotherm was successfully fitted by the Temkin equation. The sorption is spontaneous and exothermic (with reduction in maximum sorption capacity reaching up to 25 %, when temperature increases to 50 °C). Optimum platinum desorption was obtained with 0.3 M HCl solution (with solid/liquid ratio 1.67 g L^{-1}) for complete desorption and enrichment factor close to 4.6. Complete desorption was maintained over 5 cycles, while the sorption efficiency decreased by less than 3.5 % at the fifth cycle. The sorbent showed remarkable stability for PGMs (Pd(II) in addition to Pt(IV)) against alkali-earth elements or base metals (from equimolar synthetic solutions); the selectivity is driven by the preference of the reactive groups (soft base and intermediary base) for soft PGM metals against hard and borderline metal ions; this selectivity is also affected by metal speciation (formation of chloro-anionic species). The valorization of platinum from non-compliant Pt/Al_2O_3 catalyst was investigated after leaching with aqua regia. Platinum was precipitated from the leachate with ammonium chloride. In a second step, aluminum was removed by precipitation at pH 5. The residual solution was then treated by adsorption on CTTR: optimum separation between Pt and Al was achieved at pH ≈ 3.

* Corresponding authors at: IMT Mines Ales, Polymers Composites and Hybrids (PCH), 6, avenue de Clavières, F-30319 Alès cedex, France (E. Guibal) and University of South China, School of Nuclear Science and Technology, Heng Yang 421001, China (X. Yin).

E-mail addresses: m_fouda21@usc.edu.cn (M.F. Hamza), eric.guibal@mines-ales.fr (E. Guibal), yzwei@usc.edu.cn (Y. Wei), ningshunyan@usc.edu.cn (S. Ning), yinxb@usc.edu.cn (X. Yin), amr_fh83@azhar.edu.eg (A. Fouda), h.amer@tu.edu.sa (H.H. Amer).

https://doi.org/10.1016/j.susmat.2024.e01165
Received 28 August 2024; Received in revised form 15 October 2024; Accepted 31 October 2024
Available online 4 November 2024

1. Introduction

Recently Chaudhuri et al. [1] pointed out that the scarcity of PGMs in the earth-crust, combined with the growing demand (driven by High-Tech and catalytic applications), makes these metals strategic and invaluable. Therefore, it becomes urgent finding secondary sources such as urban mine (recycling of WEEE, waste from electrical and electronic equipment) or from industrial wastes (catalytic converters, etc.). Platinum is one of the precious metals (covering the list: Au, Ag, Pt, Pd, Rh, Ru, Ir and Os). Due to their high economic value, their resistance to corrosion, ductility, and poor chemical reactivity, they gained a lot of attention for applications in coining, jewelry; however, most of the demand for Pt is directed toward catalytic uses (chemical synthesis and converter for automotive emissions). Electronics industry is also consuming Pt for computer hard disks, optical fibers, LCDs. Among other less frequent uses, it is possible reporting thermocouples, turbine blades, medical devices and biomedical compounds (cisplatin and other platinum complexes). Driven by the cost of the metal around 1000 (±300) USD/oz. over the last 5 years, these applications concern high-tech and advanced industry. Strong incentives have been initiated at international and regional levels for developing politics oriented toward circular economy, including strategies for reuse of precious and strategic metals [2,3]. This is also the reason for the intense research activity for developing the valorization of infra-marginal and secondary resources [4], including the recovery of rare earth elements from industrial effluents [5] and PGMs from catalysts using in fine chemical synthesis and catalytic converters [6]. Though pyrometallurgy may be used for the recovery of PGMs from waste materials [7,8], hydrometallurgy remains the most frequent method for the removal of these metals from solid matrices, using bioleaching [9] or chemical leaching [10–12]. Generally, the leaching of spent catalysts or wastes is processed using acidic agents (HCl, or aqua regia) [13–16]. The second step in the process consists of the recovery of PGMs from leachates. The concentration levels of these valuable metals are generally high enough for allowing metal recovery and separation using solvent extraction [17–20], selective precipitation (using for example ammonium chloride for Pt precipitation [17,19,21,22]), or electrochemical deposition [23]. Residual amounts of valuable metals (at concentrations more compatible with sorption processes, meaning several hundreds of mg L^{-1}) can then be recovered using ion-exchange [24–26], extractant impregnated resin [27–29] and impregnated porous supports [30], chelating resins [31,32], and composite materials [33]. Adsorption processes are recognized for their effectiveness, cost-effectivity and readily reusability [34]. Among the wide diversity of materials to be used, the most critical criterion remains the stability of the sorbents (especially in acidic solutions), their capacity to be repeatedly synthesized (with competitive costs), fast kinetics, high selectivity. The challenge in the valorization of PGMs from waste materials consists of both the recovery of target metals from complex solutions [35], the separation of valuable metals from base metals, and the separation of the PGMs (when simultaneously present in the leachate) [36].

The current work focuses on the design of a new resin for the polishing treatment (meaning recovery of platinum from acidic solutions containing medium concentration range; i.e., 100–200 mg Pt L^{-1}). Table S1 reports several resins (or sorbents designed for the binding of PGMs) with their optimal pH (or acidity) range, maximum Pt sorption capacity, together with the reactive groups (i.e., herein centered on N- and S-bearing groups). These reactive N-sites count quaternary ammonium groups, and polyamine groups (with expected high affinity for Pt anionic species in acidic medium), while S-sites are associated with thiourea moieties or thiol groups. Platinum being part of Class B (or soft acids) shows a preference for soft ligands such as S-bearing groups (and to a lesser extent N-bearing groups) according the hard and soft acid and base theory [37–39]. The efficacy of these sorbents (Table S1) in acidic solutions was a strong incentive to the current research focusing on the synthesis of this new sorbent (i.e., CTTR) based on the controlled reaction of triallyl cyanurate with a precursor bearing a high density of sulfur groups (obtained by preliminary reaction of 5-(2-chloroethylthio)-1,3,4-thiadiazole-2-thiol with 4-methyl-5-vinylthiazole). The chemical grafting (free radical reaction) was operated in presence of AIBN (used as radical initiator). The original synthesis route involves the successive reactions of 4-methyl-5-vinylthiazole with 5-(2-chloroethylthio)-1,3,4-thiadiazole-2-thiol, and further with triallyl cyanurate (in the presence of α,α'-azoisobutyronitrile), which allows the production of a sorbent containing a high density of both N- and S-bearing groups. The diversity of amine groups (secondary, tertiary, and quaternary) offers a wide panel of acid base characteristics, which can be tailored for binding different types of platinum species. This specificity is expected to facilitate the sorption of platinum in a wide pH range, while the presence of sulfur groups brings good affinity for platinum (HSAB theory). The other merit of this work holds on the integrated treatment of real waste material (as a complementary investigation of selectivity issue from multicomponent synthetic solution).

The physicochemical properties are first characterized (using SEM, FTIR, XPS, TGA, N_2 sorption and desorption isotherms, elemental analysis and titration) for identification of the reactive groups and the porous structure of sorbent microparticles, but also for the interpretation of mechanisms involved in platinum sequestration. In a second part, the sorption properties are deeply investigated, considering the effect of pH, uptake kinetics, sorption isotherms (at fixed temperatures for evaluation of thermodynamic parameters), metal desorption and sorbent recycling, and analysis of sorption selectivity (from multielement molar concentrations). The final section is devoted to the global treatment of a non-compliant catalyst Pt/Al_2O_3, including acidic leaching, and pre-treatments for recovery of Pt and Al (successive precipitation steps with ammonium chloride (in acidic medium) and NaOH at pH 5, respectively), while the final residue is used for testing the recovery of Pt (IV) at different pH values (for optimizing the separation of Pt from Al).

2. Materials and methods

2.1. Materials

Platinum(IV) chloride (($\geq$99.9 %), 4-methyl-5-vinylthiazole (MVT; $\geq$97 %), *N*,*N*-dimethylformamide (DMF; 99.8 %), α,α'-azoisobutyronitrile (AIBN; 98 %), 2,4,6-triallyloxy-1,3,5-triazine (triallyl cyanurate, TAT; 97 %), nickel(II) chloride hexahydrate ($\geq$98 %) and zinc(II) chloride ($\geq$98 %), from Sigma-Aldrich (Merck KGa, Darmstadt; Germany). Aluminum(III) chloride (>99.0 %), calcium(II) chloride (>99.1 %), magnesium(II) chloride (95.0 %) and iron(III) chloride ($\geq$98.0 %) from Sigma Aldrich (Shanghai, China). Palladium (II) nitrate dihydrate (Pd $\geq$39.5 wt%) from Sinopharm Group Chemical Reagent Co., Ltd. (Shanghai, China). Sodium hydroxide (98.0 %), 5-(2-chloroethylthio)-1,3,4-thiadiazole-2-thiol (CETTDiazT, 98 %) and hydrochloric acid (36.46 %) were supplied by Shanghai Makclin Biochemical Co., Ltd. (Shanghai, China).

2.2. Sorbent synthesis (CTTR)

For the quaternization reaction of 4-methyl-5-vinylthiazole, 6.25 g (50 mmol) of MVT and 10.64 g (50 mmol) of CTTDiazT were dissolved in 30 mL of DMF solution. The reagents were mixed under nitrogen atmosphere for 5 h at 21 °C, before raising the temperature to 50 °C, for another 5 h period. After cooling to room temperature, a mixture of AIBN (0.16 g, 1 mmol) and TAT (4.16 g, 11.64 mmol) dissolved in DMF (20 mL) was added dropwise. The temperature of the mixture was raised again to 65 °C for 5 h to finalize the production of CTTR (19.71 g; >98 %) as a yellow precipitate (that was washed with acetone and air-dried at 50 °C for 12 h). Scheme 1 reports the suggested synthesis route for the preparation of CTTR (adaptation of a synthesis procedure described for the quaternization of 4-vinyl-pyridine-co-acrylamide, [40]).

2.3. Sorbent characterization

Morphology (size and shape) of the sorbent was characterized using Phenom ProX scanning electron microscope (Thermo-Fisher Scientific, Eindhoven, Netherlands). The SEM is equipped with energy dispersive X-ray tool (EDX) for semi-quantitative EDX analysis of elements at the surface of the sorbent. The nitrogen adsorption desorption isotherms were acquired on Micromeritics TriStar-II high throughput surface area and porosity analyzer (Norcross, GA, USA), operated at 77 K. The sorbent was first degassed under N_2 for 5 h at 110 °C. The BET method was used for calculating specific surface area (S_{BET}), while porous characteristics were calculated by the BJH method. Thermal degradation tests were performed with TGA analyzer under nitrogen atmosphere (STA-449 F3; Jupiter Netzsch, Gerätebau HGmbh-Selb, Germany); the temperature ramp was set to 10 °C min^{-1}. XPS (x-ray photoelectron spectroscopy) was applied for characterizing the structure of the sorbent and its interaction with platinum using ESCALAB-250XI+ (Thermo Fischer Scientific Inc., Waltham, MA, USA); Al K_α monochromatic radiation was used at binding energy of 1486.6 eV, under 10^{-8} mbar pressure; the spot-size was 500 μm. The calibration was performed on C 1s signal (for C—C, $C_{adv.}$) at the binding energy, BE, of 284.8 eV. The samples (pristine sorbent, after test with simulated loading solution, after loading with metal ion, and after elution for 5 cycles) were dried, grinded with KBr, and packed under pressure to form disks for Fourier-transform infrared spectroscopy (FTIR). The analysis was achieved through IR-Tracer100 spectrometer (Shimadzu Corporation, Tokyo, Japan). The pH of zero charge (pH_{pzc}) was determined through the pH drift method using 0.1 M NaCl as salt background. A fixed amount of sorbent was dropped into a series of flasks of saline solutions at different pH *v*alues (pH_0: 1–11). The flasks were agitated for 48 h and the equilibrium pH (pH_{eq}) was measured. The pH_{pzc} corresponds to the value of pH giving $pH_0 = pH_{eq}$. The pH of the solution was initially adjusted, and the final pH measured using S220-Seven pH-ionometer (Mettler Toledo, Shanghai, China). The elemental composition of the sorbent was determined using a *V*ario EL cube (Elementar Analysen systeme GmbH, Langenselbold, Germany).

2.4. Sorption tests

Sorption tests were performed in batch by mixing (at v: 210 rpm), a fixed amount of sorbent (m, g) with a volume of solution (*V*, L) at given metal concentration (C_0, mmol L^{-1}) and fixed initial pH_0. At equilibrium time (or given contact time for kinetic experiments), samples were withdrawn and filtrated (using a filter membrane - 1.2 μm pore size) for analyzing residual metal concentration (C_{eq}, mmol L^{-1}). The metal concentration was analyzed using ICPS,7510 inductively coupled plasma atomic emission spectrometer (Shimadzu Corporation, Kyoto, Japan). The pH of the solution was not adjusted during the sorption but the final pH (pH_{eq}) was systematically recorded. The mass balance equation was used for calculating the sorption capacity (q_{eq}, mmol g^{-1}): $q_{eq} = V \times (C_0\text{-}C_{eq})/V$. Experiments were duplicated and the average value was used (error bars are represented in figures). The same procedure was applied for investigating Pt(IV) sorption from multi-component solutions.

For desorption tests, Pt-loaded sorbent was collected from uptake kinetic experiments. The rinsed samples were dried and mixed (also in batch) with the eluent for given contact times. The concentration in the eluate was analyzed and the efficiency of desorption was calculated by the mass balance equation. For the study of sorbent recycling, a water rinsing step was systematically processed between the different sorption and desorption steps.

Experimental conditions are systematically (briefly) reported in the caption of the Figures. The temperatures were controlled at fixed values (with a possible variation of ±1 °C); values reported in the caption are reported at theoretical fixed values (for practical editing).

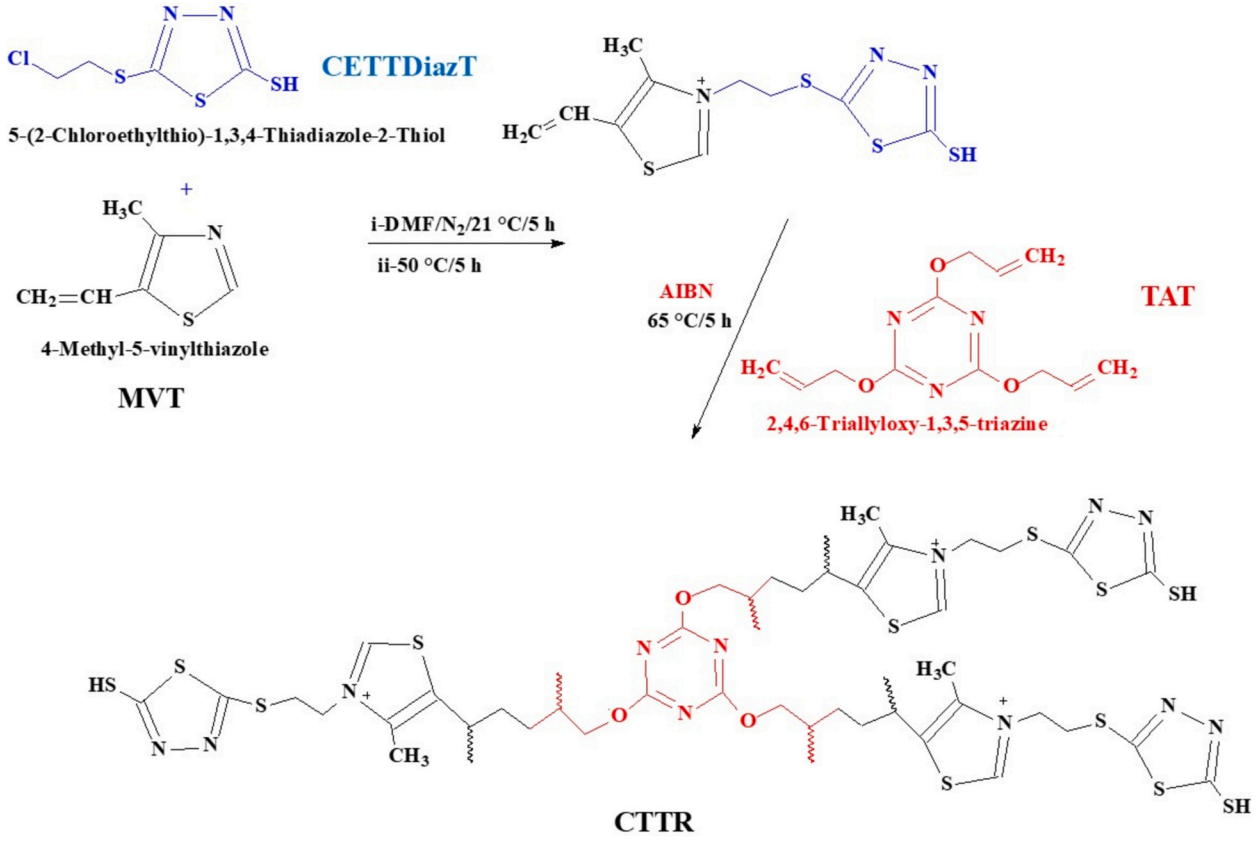

Scheme 1. Synthesis route for the preparation of CTTR.
Synthesis - Check Atta et al. (2019) [40].

The modeling of experimental data was performed using nonlinear regression analysis and the facilities of Mathematica ® (and proprietary notebooks) for the determination of relevant parameters. The quality of the fits was calculated by the determination coefficient (i.e., R^2) and the Akaike information criterion (AIC, [41]). The equations used for modeling uptake kinetics and sorption isotherms are summarized in Tables S2a and S2b, respectively.

2.5. Application to platinum recovery from valorization of non-compliant catalysts

The sample of non-compliant catalyst (grinded, and the obtained particle size ranged around 1–0.5 mm) was leached using aqua regia (HCl/HNO_3: 3:1) at T: 75 °C (to enhance leaching efficiency) for 1 h. The solid/liquid (S/L) ratio was 1:3 (i.e., 1 kg catalyst for 3 L of aqua regia). The volume of leachate collected in this step reached 2.75 L.

First, Pt was precipitated from leachate using 30 g L^{-1} NH_4Cl at pH 0.9 (±0.1) (1 L of the leachate solution consumed 100 mL of ammonium chloride solution).

The pH of the solution kept in acidic medium by HCl to avoid formation of NH_3 and support formation of $(NH_4)_2PtCl_6$ complex. Platinum precipitation exceeded 92 % under these experimental conditions. The produced residue was used for further extraction using CTTR sorbent at different pH values. The concentration of the main elements was 21,716, 0.89, and 151 mg L^{-1} for Al, Ti, and Pt, respectively.

Due to the huge excess of aluminum compared to Pt (with strong competition and effect of high salinity), another solution was prepared by pre-treatment of the leachate involving pH control to 5 (for aluminum precipitation, the solution became turbid at pH_0 3 and above). After filtration, the pH 5 solution was adjusted to different pH values (in the range pH_0 1–5) for investigating sorption onto CTTR.

The sorption process was applied by contact of 100 mL of solution with 1 g of CTTR at different pH_0 values (in the range 1.01–5.02) for 1 h, under agitation (v: 210 rpm), at room temperature (i.e., T: 21 °C).

3. Results and discussion

3.1. Characterization of sorbent

3.1.1. SEM observation and textural properties

Fig. S1 shows SEM micrographs of the sorbent. The average size of the particles is close to 6.4 ± 0.8 μm. The morphology of the sorbent can be defined as a packing of different types of objects: fluffy platelets, smoothed rounded particles, and squared objects with sharp edges. This structure may contribute to expended external surface area. In Fig. S1c, the SEM photograph of the sorbent after recycling does not show substantial difference (compared with initial CTTR sorbent, Fig. S1a,b). The N_2 adsorption and desorption isotherms (shown in Fig. S2a) allow calculating the specific surface area (close to 59.2 m_2 g^{-1}), using BET equation. This type of profile combines Type IV and Type I isotherms according IUPAC classification. Chen et al. [42] reported similar N_2 adsorption/desorption isotherms (Type I/IV profile), for hierarchically porous carbon microfibers; they identified the coexistence of micro- (0.74 nm) and mesopores (2.1–3.9 nm). Wu et al. [43] also claimed for mushroom waste biochar that this type of profile corresponds to mixed Type I and Type IV isotherms with presence of micropores and mesopores. On the opposite hand, Zhang et al. [44] assigned to the similar isotherm a Type IV profile, which was associated with a mesoporous structure for zinc-nickel-cobalt oxide microspheres (with dual distribution of pore sizes: around 12 nm and a smaller fraction of small pores at ≈3 nm). Tang et al. [45] reported similar N_2 adsorption/desorption isotherm for ZIF (zeolitic imidazolate framework) sorbent. The initial steep section of the curve ($p/p_0 < 0.1$) can be assigned to the contribution of micropores, while the hysteresis loop can be attributed to a sharp capillary step within an array of ordered uniform mesopores. The BJH equation was used for analyzing porous characteristics. Herein, there is a narrow distribution of pores close to 3 nm considering the adsorption branch, while the desorption branch shows a broader pore size distribution (Fig. S2b). The porous volume is evaluated in the range 0.0445–0.0487 cm^3 g^{-1} (depending on the adsorption and desorption branches).

3.1.2. TGA

The weight loss in TGA shows 4 transitions (Fig. S3):

(a) 27.3–237.0 °C: Water release (Weight loss, WL: 19.2 %)
(b) 237.0–509.2 °C: WL reaches 50.6 %, with strong dTG (differential thermogravimetry) peak at 488.7 °C and weaker dTG peaks at lower temperatures (i.e., 273.2 °C and 330.6 °C),
(c) 509.2–661.6 °C: a new WL is observed representing 11.6 %, and.
(d) 661.6–803.6 °C: the WL (does not exceed 6.8 %), with weak dTG at 693.4 °C.

The residue after thermolysis, under N_2 atmosphere, represents about 11.7 % (in weight).

Similar trends were reported for the thermal degradation of composite materials incorporating the precursors (or analogues) used for the synthesis of CTTR. Hence, Sharma and Singh [46] reported 3 waves in the thermal degradation (under air atmosphere) of a composite associating SBA-15 and 2,4,6-triallyloxy-1,3,5-triazine (TAT) with exothermic peaks at ≈300, 400 and 480 °C. In the case of polystyrene functionalized with mercapto-derivative of thiadiazol, the decomposition occurred in two main steps: (a) 40–280 °C (WL: about 14.1 %) and 280–500 °C (WL: about 63 %), while at 600 °C the residual mass did not exceed 21 % [47] (comparable to the residue obtained with CTTR) [47]. Madani et al. [47] concluded that the functionalized sorbent is thermally stable. Dani et al. [48] investigated the thermal degradation of 5-methyl-1,3,4-thiadiazole thiol (close to CETTDiazT precursor) [48], under nitrogen atmosphere: they observed three waves. The compound does not lose weight below 190 °C (no water release), while between 190 °C and 500 °C the material is almost fully decomposed (about 97 %, total degradation occurs at 750 °C). The other substituents on the compounds (as those on CETTDiazT) and the reaction with other precursors contribute to the reinforcement of the stability of the sorbent. The thermal degradation of 5-amino-1,3,4-thiadiazole-2-thiol-grafted silica gel is characterized by 3 transitions with peaks identified at 50 °C, 240 °C, and 340 °C: below 280 °C the composite lost 22 %, and about the same amount between 280 °C and 900 °C.

3.1.3. FTIR analysis

The FTIR spectrum of CTTR is characterized by a series of typical bands representative of the signals present in the precursors (MVT and CETTDiazT) (Fig. S4, Table S3). Hence, N-bearing groups are detected at 3422 cm^{-1} (associated with the overlapping of ν_{N-H} and ν_{O-H}, probably attributed to the hydration of the sorbent) (secondary heterocyclic amine, resulting from partial tautomerization); 1612 cm^{-1} ($\nu_{C=N}$ and/or δ_{N-H}), 1549 cm^{-1} (conjugating several contributions: $\nu_{C=N}$, ν_{C-N}, marker of triazine ring skeleton), 1458 cm^{-1} (ν_{C-N}). S-based moieties are identified by the bands at 2567 cm^{-1} (ν_{S-H}), and 627 cm^{-1} (ν_{C-S}). The incorporation of TAT is characterized by the presence of signals associated with C-O-C bands at 1356 cm^{-1} (ν_{C-O}), 1271 cm^{-1} (ν_{sC-O-C}), and 1128 cm^{-1} ($\nu_{asC-O-C}$) and other markers of triallyl cyanurate (TAC) such as the band at 1458 cm^{-1} (attributed to ν_{C-N} and δ_{C-H} in methylene). Other bands (or shoulders) are assigned to aliphatic chains (1385, 827, and 773 cm^{-1} for δ_{C-H}), and ν_{C-H} vibration on the range 2970–2880 cm^{-1}.

FTIR spectrometry can be also used for approaching the modes of interaction of the sorbent with metal ions (Fig. 1). The sorption of Pt(IV) is operated in acidic solutions, which may affect the protonation of some reactive groups (and provoke tautomerization effects). To identify more clearly the relative contributions of sorbent protonation and the proper interaction of the sorbent with Pt(IV), the CTTR spectrum is compared

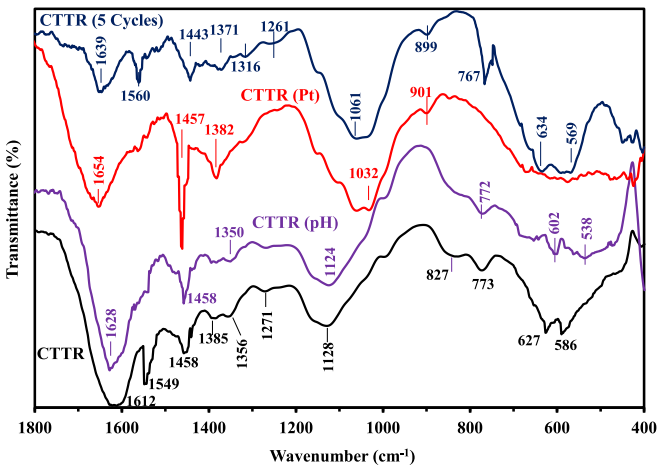

Fig. 1. FTIR spectra of the sorbent under different states: sorbent as produced (CTTR), after pH control (CTTR (pH)), after Pt(IV) sorption (CTTR (Pt)), and after 5 cycles of re-use (CTTR (5 cycles)) (1800–400 cm^{-1} wavenumber range).

with the spectra after treatment at pH 4 (CTTR (pH)) and after metal sorption (CTTR (Pt)). The protonation of the sorbent essentially influences the band at 1549 cm^{-1} that almost disappears after conditioning at pH 4 (being replaced with a shoulder). The formation of supplementary protonated sites induces the tautomerization of relevant reactive groups (Scheme S1, Supplementary Information). The modification of the environment of N-bearing groups is confirmed by the significant shift of the band at 1612 cm^{-1} that moves to 1628 cm^{-1}. The sorption of Pt(IV) induces larger changes in the FTIR spectrum. The band at 3422 cm^{-1} is significantly broader with a shift toward lower wavenumber (i.e., 3389 cm^{-1}): the binding of platinum (as chloroanionic species) involves interaction of N-based reactive groups. The $\nu_{C=N}$, δ_{N-H} vibrations (at 1621 → 1628 cm^{-1} after protonation) are displaced toward higher wavenumber (i.e., 1654 cm^{-1}). The intensity of the band at 1382 cm^{-1} significantly increases (associated with δ_{C-H} in methylene): this is probably due to the modification of the chemical environment of methylene group (rather than the direct interaction of platinum onto methylene groups). It is noteworthy that the band at 1128–1124 cm^{-1} (assigned to $\nu_{asC-O-C}$, and TAC marker) is drastically shifted by almost 100 cm^{-1} after Pt(IV) sorption (toward 1032 cm^{-1}): the allyl cyanurate ring in TAT is significantly perturbated (tautomerization and metal binding on N-bearing groups). In addition, the broad band at 2567–2573 cm^{-1} (assimilated to a doublet for ν_{S-H}) is replaced with a well-defined single peak (at 2562 cm^{-1}); meaning that S- functional groups are also involved in platinum binding. This is also confirmed by the strong weakening of the band at 627 cm^{-1} (as ν_{C-S}, moved to 602 cm^{-1} after protonation, with intensity reduction), which almost disappears (stronger variation compared with simple protonation): S-based reactive groups contribute to platinum sorption. The band at 773–772 cm^{-1} (δ_{C-H}) is no more detected after Pt(IV) binding. A weak band is detected at 901 cm^{-1}; similar weak signal was reported after lead adsorption onto 5-amino-1,3,4-thiadiazole-2-thiol grafted silica [49].

After desorption and sorbent reuse (for 5 successive cycles), the FTIR spectrum is partially restored (Fig. 1). However, some remarkable changes can be observed: (a) the broad band at 3414 cm^{-1} is not completely restored (initially at 3422 cm^{-1}), (b) a shoulder appears at 1725 cm^{-1} (attributable to $\nu_{C=O}$), (c) shift of 1612 cm^{-1} band ($\nu_{C=N}$) toward 1639 cm^{-1}, (d) shifts in the band at 773, 627, and 586 cm^{-1} (toward 767, 634, and 569 cm^{-1}) with disappearance of the band at 827 cm^{-1}, and (e) the band at 1128–1124 cm^{-1} remains shifted to 1061 cm^{-1} (consistently with the displacement observed after Pt(IV) sorption). This means that the recycling of the sorbent induces significant changes in the structure, probably associated with the chemical modification of some reactive groups (appearance of C=O group), irreversible shift of $\nu_{asC-O-C}$ band, and modification of the environment of C=N groups. It is noteworthy that the loss in sorption performance at recycling remains negligible at the fifth cycle (see Section 3.2.6.); this means that despite the chemical modification of some groups the sorption properties are not significantly impacted.

3.1.4. XPS analysis

The XPS survey spectra of CTTR before and after Pt(IV) sorption are reported in Fig. 2. CTTR material is characterized by the presence of the signals of C 1s (at binding energy, BE: ~285 eV), N 1s (~400 eV), O 1s (~532 eV), and S 2p (~168 eV) (with S 2s at 270 eV). Traces of chlorine are also detected at 199 eV (Cl 2p) and 225 eV (Cl 2s); meaning that CETTDiazT was not fully grafted or converted in the synthesis of CTTR sorbent. After Pt(IV), the same signals are observed with almost the same BEs (variations by less than 1 eV), with appearance of bands associated with Pt 4f signal (at ~72 and ~ 75 eV, for Pt $4f_{7/2}$ and Pt $4f_{5/2}$, respectively), Pt 5s (at ~103 eV), and Pt 4d (at ~311 and ~ 334 eV for Pt $4d_{5/2}$ and Pt $4d_{3/2}$, respectively). The determination of the chemical structure of CTTR and the interpretation of its interactions with Pt(IV) can be completed by the discussion of high-resolution XPS spectra (HRES XPS spectra, Fig. S5). The reaction and grafting of the three precursors to produce CTTR leads to the coexistence of a wide diversity of functional groups that makes difficult the assignment of the different signals (deconvoluted bands with superposition of contributions): Table S4 suggests possible assignments based on literature survey. The interpretation of XPS spectra and the assignments of deconvoluted bands is made complex by the effects of tautomerization in the following groups N=C-SH, N-N=C, S-C=N and in the heterocyclic ring (triazine). The most interesting information to be extracted from these analyses concerns the impact of Pt(IV) sorption on the deconvoluted components (in terms of BEs and atomic fractions, AFs). The global observation of HRES-XPS spectra shows that the most significant changes are related to C 1s (reinforcement of the ~286.2 eV band probably associated to C—N, C—O, and C-O-C bond, and decrease of the intensity of the ~289 eV, assigned to O-C=N and/or O-C-N bonds), N 1s (appearance of the band at ~399.7 eV, attributed to N—Pt bond), and S 2p (weak decrease of the intensity of S 2p in C-S-C and little increase for -SH bond with shift in BE by −1.5 e*V*, for S $2p_{3/2}$ and S $2p_{1/2}$ spin-orbit components). This means that platinum sorption involves N-based and S-based (preferentially sulfhydryl groups, -SH) functional groups; the occurrence of tautomerization effects contributes to the delocalization of double bonds and transfer of charges (Scheme S1). This means that some complementary chemical groups may be formed, including quaternary ammonium groups (with affinity for chloroanionic platinate species).

Another important information may be deduced from the analysis of

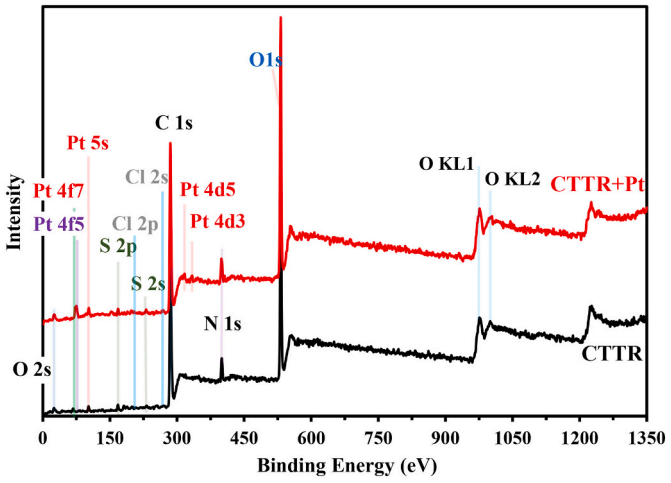

Fig. 2. XPS survey spectra for CRRT before and after Pt(IV) sorption.

Pt 4f signal (Fig. S5, Table S4). The signal can be deconvoluted into 4 components corresponding to 2 spin-orbit doublets (Pt $4f_{7/2}$ and Pt $4f_{5/2}$, respectively) corresponding to Pt(IV) (at ~74.5 eV and ~ 77.8 eV) and Pt(II) (at ~72.4 eV and ~ 75.7 eV) forms [50,51]. The fraction of Pt(IV) reduced to Pt(II) represents up to 72.5 %: after hexachloroplatinate sorption, the metal is substantially reduced. The normal redox potential of $PtCl_6^{2-}/PtCl_4^{2-}$ is weak (close to 0.726 V [52]). This may explain the easy reduction of the metal in mild acid solution and in the presence of organic sorbent. The sorbent and sorption medium (mild acidic conditions) both support the reduction of Pt during extraction process; this is also clearly confirmed by XPS analysis. The discussion of high-resolution XPS spectra shows (a) the deconvolution for O 1 s, N 1 s and S 2p signals with significant changes in the FWHM and atomic fraction (%) after Pt sorption, and (b) the coexistence of different bands for Pt 4f signal (proving the coexistence of different oxidation states). Mild acidic solution provides favorable conditions for electron donation (available on the chelating atom) to Pt(IV) ions (electron acceptor). Oxidizing groups, mainly as amine and thiol groups in CTTR, (which are grafted on the polymer backbone during synthesis or which result from tautomerization mechanisms) support the reduction process of Pt. The HRES XPS spectra show the presence of thiol groups (due to tautomerization effect). This was also favored by the heterocyclic bi-bond. This band slightly increases after Pt sorption; this is accompanied by some shifts in binding energy: for CTTR, the two peaks at 164.01 and 165.19 eV (with AF%: 3.11 and 1.56 respectively), are shifted to 162.49 and 163.67 eV after metal sorption (with AF%: 5.73 and 2.86 % respectively). These changes cause the increasing in the AF% of thiol groups combined with changes in amine moieties (including formation of quaternary ammonium groups, QA). This is confirmed by (a) the increase in AF% for QA, and (b) the decrease of secondary and tertiary amine peaks. Hence, the peak at 399.32 eV (with AF%: 51.35 %) was shifted to 398.68 eV (with decreasing AF% to 36.08 %). This is probably related to the oxidation of some amine groups to QA (secondary and tertiary amine may lose electron, behaving as reducing agent, resulting in a partial oxidation, associated with the changes in intensity and BEs of relevant groups). This interpretation is consistent with the discussion of Pt 4f signal. The deconvoluted peaks show 4 components corresponding to 2 spin-orbit doublets for Pt(IV) (at ~74.5 eV and ~ 77.8 eV) and Pt(II) (at ~72.4 eV and ~ 75.7 eV) forms.

3.1.5. Elemental analysis and pH_{pzc}

The elemental analysis confirms the high densities of N and S elements in CTTR (Table S5): 8.92 mmol N g^{-1} and 9.32 mmol S g^{-1}. The theoretical N/S ratio (based on the expected structure of CTTR) is 1:1, consistently with the elemental analysis (i.e., 0.96:1). On the opposite hand, oxygen is in large excess compared with theoretical molar ratio: O/N (and O/S) should be closed to 1:4, meaning molar content close to 2.25 mmol O g^{-1}, while the analysis gives a content close to 7.44 mmol g^{-1}. This excess of O is probably due to the absorption of H_2O.

Fig. S6 shows the determination of the pH_{pzc} using the pH-drift method, with two different concentrations of the background salt: 0.1 M and 1 M NaCl. The pH_{pzc} values varies between 4.52 and 4.77, respectively. The sorbent surface is positively charged in acidic solution (at pH below 4.6). The maximum pH changes are observed around pH_0 3 (corresponding to the highest protonation of CTTR surface). Above pH 3, the surface charge decreases up to pH_{pzc}, where the surface charge is totally neutralized. It is noteworthy that in 1 M NaCl solutions the screening effect of Na^+ reduces the surface charge (compared with 0.1 M NaCl solution). The precursors MVT and TAT have low predicted pK_a values (i.e., 3.17 ± 0.10 and 2.04 ± 0.10, respectively). The synthesis of CTTR with crossed grafting may obviously change the acid-base properties of relevant functional groups, leading to substantial shift of global pH_{pzc}. This shift may be also influenced by the tautomerization mechanisms (illustrated by Scheme S1).

3.2. Pt(IV) sorption – synthetic solutions

3.2.1. pH effect

Fig. 3 compares the effect of the pH on Pt(IV) sorption at two different temperatures. The sorption is exothermic: the sorption capacity significantly decreases with increasing the temperature. At low pH (i.e., pH ~1), the competition of chloride ions strongly reduces the sorption capacity (below 0.08 mmol Pt g^{-1}). With the increase of the pH, the sorption progressively increases (especially for $pH_{eq} > 2$) before stabilizing above pH_{eq} 3.5. The protonation of the sorbent and the competition of chloride counter anions decrease, explaining the enhancement of platinum sorption. In addition to the protonation effect, the speciation of Pt(IV) in HCl solution is controlled by the pH of the solution: At pH 1, platinum is predominantly present as H_2PtCl_6 with coexistence of $HPtCl_6^-$ [53]. Spieker et al. [54] deeply investigated by EXAFS the distribution of chloroplatinic acid in aqueous solutions and they highlighted the importance of ligand exchanges (chloride, hydroxide ion) in function of the pH, the concentrations of metal and chloride ion, or light irradiation. This makes the chemistry of platinum in solution relatively complex (including considering proper kinetics of ligand exchange). When the pH increases the proportion of $HPtCl_6^-$ increases (reaching a maximum at pH 2, about 80 %), $PtCl_6^{2-}$ and $PtCl_5(H_2O)^-$ also appear. The maximum of these species is reached at pH 3.5, representing ~10 % and ~ 46 %, respectively, $HPtCl_6^-$ is still present at this pH (~12 %), while $PtCl_4(H_2O)(OH)^-$ appears (up to ~32 %). At pH 4, hydrolyzed and hydrated species predominate ($PtCl_4(H_2O)(OH)^-$ and $PtCl_5(H_2O)^-$ represent ~56 % and ~ 34 %, respectively). At pH 5.8, platinum is present only as $PtCl_4(H_2O)(OH)^-$; where colloids may exist with precipitation. Platinum sorption on CTTR is favored by the increasing predominance of non-hydrolyzed anionic species (up to pH_{eq}: 3.5), while the predominance of hydrolyzed species (i.e., $PtCl_4(H_2O)(OH)^-$) leads to the stabilization of metal sorption. The effect of metal speciation is reinforced by the influence of the protonation of reactive groups. The pHpzc of the sorbent is found close to 4.6 ± 0.1. In the whole tested pH range, the surface remains positively charged and available for the binding of anionic platinum species. The direct interpretation of the pK_a values of associated functional groups is made complex by the parallel mechanisms of tautomerization (which affects the intrinsic dissociation of specific reactive groups). It is also noteworthy that the coexistence of different types of amine groups tends to widen the pH range corresponding to the protonation of N-bearing sites. Sorption tests were not performed above pH 4 to prevent possible phenomena of metal precipitation. Iglesias et al. [55] commented that for sorbents bearing N-

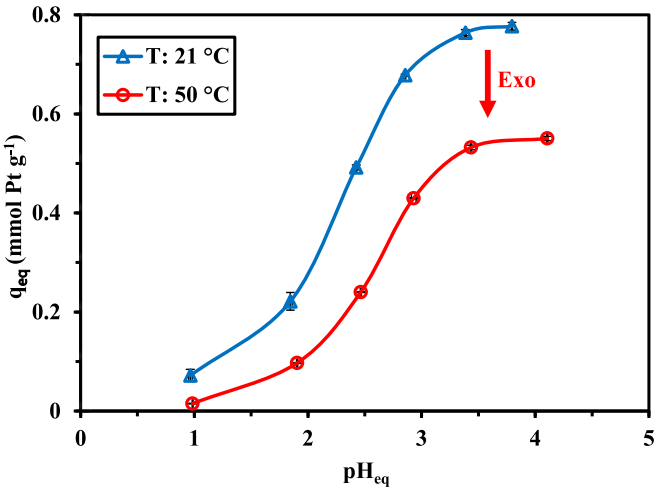

Fig. 3. Effect of pH on Pt(IV) sorption capacity using CTTR at T: 21 °C and 50 °C (Sorbent dose, SD: 0.333 g L^{-1}; C_0: 0.266 mmol Pt g^{-1}; v: 220 rpm; time: 48 h).

groups, the sorption of metal chlorocomplexes may operate through two mechanisms: anion-exchange when the sorbent is protonated (ion-exchange of counter anion with chloroplatinate species) or chelation of metal anion by coordination onto free nitrogen. The efficient sorption of Pt(IV) is then controlled by the protonation of N-groups balanced by the excess of counter anions (i.e., chloride anions) and the reactivity of thiol groups in acidic solutions. At higher pH values, the competition of counter anions decreases, while the N-groups remain protonated (up to pH 3.5); this makes the sorption becoming more efficient with the supplementary contribution of thiol groups. Dobrowolski et al. [56] reported similar increase in sorption performance with a maximum reached between pH 1 and 3: increasing the number of grafted amine groups shifted the pH-edge curve toward higher pH values. Above pH 4 sorption tended to decrease due to the lower affinity of the reactive groups for predominant $PtCl_5(OH)^{2-}$ and $PtCl_4(OH)_2^{2-}$ species.

Fig. S7a shows that the sorption process hardly changes the pH of the solution. Actually, pH slightly decreases, by less than 0.1 pH unit, regardless of the temperature. However, at pH 4, a slight difference is observed between T: 21 °C (pH decreases by 0.2 unit) and T: 50 °C (pH increase by 0.1 unit). The slight pH decrease can be related to the binding of platinum through proton release; this effect may be also reinforced by the tautomerization of the thiadiazol ring (which withdraws electrons from S bearing groups and releases protons, which, in turn, decreases the final pH), and/or the binding of $PtCl_4(H_2O)(OH)^-$ (at least in the pH range 3–4). The distribution ratio (as $\log_{10}$ D, $D = q_{eq}/C_{eq}$) is plotted vs. pH_{eq} for the two experimental series in Fig. S7b. For T: 21 °C, experimental data linearly align with a slope close to 0.94. This slope is usually associated in ion exchange reaction to the stoichiometry of proton exchange. Herein, the sorption process may proceed through electrostatic attraction of chloroanionic platinate species onto protonated reactive groups and by chelation on free amine groups and S-based groups. This slope may thus be taken with caution. At T: 50 °C, the same trend is followed (slope close to 1); however, a slope breakthrough can be observed when pH_{eq} exceeds 3. This confirms the negative effect of temperature on sorption performance, especially at pH above 3.

Neagu et al. [57] synthesized functionalized acrylic copolymers bearing either amidoethylamine groups or thiol groups; the method involving the aminolysis-hydrolysis of ethylenediamine, produces the most efficient sorbent (compared with thiol bearing sorbent, prepared with thiourea). The sorption of Pt(IV) decreased progressively with increasing the pH (from pH 1 to 5). The functionalization (with dimethylamine) of cross-linked lignophenol produced an efficient sorbent with high efficiency for Pt(IV) recovery from strong acid solutions ([HCl] ~1–5 M) [58]; this sorbent was less sensitive to strong acid solutions than CTTR. In the case of chitosan beads doped with polyethyleneimine, the sorption of Pt(IV) decreased when the concentration of HCl exceeded 0.1 M (remaining almost constant between pH 2 and 1) [50]. In the case of sulfoethylated amino polymers, the optimum sorption was found close to 1.6: at stronger acidity the competition effect of Cl^- anions limited the sorption, while above pH 1.6 the decrease of the protonation of amine groups decreased the reactivity of the sorbent [59]. The effect of pH on surface charge may be reinforced by the progressive change in the speciation of platinum in solution (decrease of the $PtCl_6^{2-}$ fraction) [60]. In the case of Pt(IV) sorption onto polyethyleneimine-functionalized non-woven fabrics (polyethylene/polypropylene), Feng et al. [61] found an opposite trend (which is consistent with the results collected with CTTR): sorption increased from pH 1 to 3 and stabilized above. $PtCl_6^{2-}$ was also the preferred Pt(IV) species in the case of PEI-functionalized polystyrene beads, while reaching a maximum at pH 2 [26].

Further experiments are performed at optimum pH_0 4, with a sorbent that maintains (a) a surface positively-charged, (b) a minimized competition of chloride anions (for ion exchange of platinum anionic species with chloride anion) and (c) the presence of appropriate hexachloroplatinate species (i.e., $PtCl_6^{2-}$ and associated species).

3.2.2. Uptake kinetics

The kinetics of sorption are represented in Fig. 4. Under selected experimental conditions (i.e., C_0: 0.258 mmol Pt L^{-1} = ~50 mg Pt L^{-1}; pH_0: 4; SD: 0.333 g L^{-1}), the equilibrium is reached in 30–40 min, regardless of the temperature (i.e., 21 °C vs. 50 °C). The half time of sorption (corresponding to the time required for q(t) achieving half of the equilibrium sorption, q_{eq}) is almost equivalent to ~12 min at T: 21 °C and 50 °C. However, consistently with Fig. 3 and the exothermic nature of the sorption process, the residual concentration is significantly higher at T: 50 °C (0.078 mmol Pt L^{-1}) than at T: 21 °C (0.0077 mmol Pt L^{-1}); corresponding to sorption capacities at equilibrium close to 0.536 mmol Pt g^{-1} and 0.750 mmol Pt g^{-1}, respectively. The kinetics may be controlled by mechanisms such as (a) resistance to film diffusion and intraparticle diffusion, considering the ionic size of the sorbate but also the porous characteristics of the sorbent (and particle size), and operational parameters such as the agitation speed, and (b) intrinsic reaction rate (which is frequently associated with pseudo-first or pseudo-second order rate equation; PFORE and PSORE, respectively). In Fig. 4, the solid lines represent the fits of experimental data with the PFORE. Globally, the modeled lines superpose to experimental point with little discrepancies in the 25–40 min range (higher curvature zone). However, Figs. S8 and S9 show that the PSORE and the Crank equation (for resistance to interparticle diffusion equation) exhibit even higher discrepancies. This is also confirmed by Table 1, where the parameters of the models (together with statistical criteria: R^2 and AIC) are summarized. The PFORE reaches much better statistical indices; in addition, the calculated equilibrium sorption ($q_{eq,1}$) for PFORE is much closer (over-estimation by less than 4 %) for experimental value than PSORE (overestimation by 18–19 %). The apparent rate coefficient (k_1) is hardly influenced by the agitation (ranging between 0.066 and 0.070 min^{-1}). The comparison with other sorbents is made difficult by different experimental conditions; in addition, in many cases, the pseudo-second order rate equation fits better experimental data. Chaudhuri et al. [60] obtained k_1 value close to 0.141 min^{-1} while using graphene oxide-dendritic sorbent. In the case of chitosan functionalized with DB18C6 (dibenzo-18-crown-6-ether), the apparent rate coefficient increased with temperature in the range 0.0031–0.0113 min^{-1} [28]. For Pt(IV) biosorption using tannins extracted from *Terminalia cattapa* L. leaf, the rate coefficient increased with temperature from 0.014 to 0.042 min^{-1} (between 20 °C and 50 °C) [62]. Xue et al. [63] functionalized graphene-polyurethane composite with cysteine moieties: the apparent rate coefficient is evaluated to 0.194 min^{-1}. Contrary to these examples, the sorption of Pt(IV) on aminated magnetic silica nanoparticles was best fitted by the PFORE and the apparent rate coefficient was close to 2.60 min^{-1} (i.e., more than 100-fold the k_1 value for

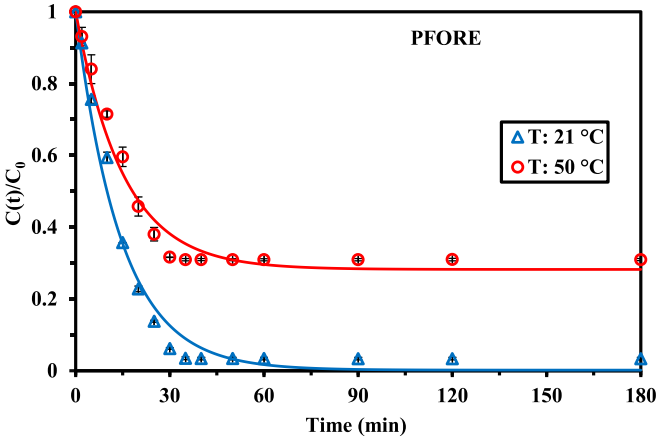

Fig. 4. Pt(IV) uptake kinetics using CTTR at T: 21 °C and 50 °C – Pseudo-first order rate equation fits (C_0: 0.258 mmol Pt L^{-1}; pH_0: 3.99, pH_{eq}: 3.81 at 21 °C and 4.12 at 50 °C; SD: 0.333 g L^{-1}; v: 220 rpm).

Table 1
Pt(IV) uptake kinetics – Parameters of the models.

Model	Parameter	Unit	Temperature	
			21 °C	50 °C
Experimental	$q_{eq,exp}$	mmol g^{-1}	0.750	0.536
PFORE	$q_{eq,1}$	mmol g^{-1}	0.775	0.557
	k_1	min^{-1}	0.0696	0.0659
	R^2	–	0.987	0.981
	AIC	–	−90	−95
PSORE	$q_{eq,2}$	mmol g^{-1}	0.886	0.639
	k_2	g $mmol^{-1}$ min^{-1}	0.100	0.130
	R^2	–	0.951	0.943
	AIC	–	−71	−79
RIDE	$D_e \times 10^{14}$	m^2 min^{-1}	0.84	5.23
	R^2	–	0.959	0.946
	AIC	–	−66	−78

D_0 ($PtCl_6^{2-}$): 0.79 × 10^{-5} cm^2 s^{-1} = 4.74 × 10^{-8} m^2 min^{-1} [65].

Amberjet 4200 (a commercial resin bearing quaternary ammonium salt groups) [64]. The imprecise fit of experimental profiles with the RIDE can only be used for giving an order of magnitude for the effective diffusivity (D_e) around 0.84–5.23 × 10^{-14} m^2 min^{-1}. Surprisingly, the diffusion coefficient would be higher at 50 °C contrary to the little faster sorption at 20 °C; this is due to the inappropriateness of the simple diffusion model for describing the experimental curves. In any case, this range of values is several orders of magnitude lower than the free diffusivity of $PtCl_6^{2-}$ in water (i.e. 8.4 × 10^{-8} m^2 min^{-1}, [65]). The contribution of the resistance to intraparticle diffusion cannot be neglected; this may be associated with the inaccuracy of the PFORE fit in highly curved zone of the kinetic profile.

Fig. S10 shows the influence of increasing Pt(IV) concentrations on uptake kinetics using CTTR. The equilibrium time is not significantly affected by changing the concentration: the equilibrium is systematically achieved in ≈35 min. The modeling of kinetic profiles is reported in Table S6. The apparent rate coefficient for PSORE (i.e., k_2, g $mmol^{-1}$ min^{-1}) linearly decreases with increasing the concentration of platinum (k_2 = 0.112–0.0436 [Pt] with R^2: 0.9996) (Table S6). On the opposite hand, in the case of PFORE, the apparent rate coefficient does not follow a continuous trend: k_1 varies around the average value 0.072 (±0.008) min^{-1}. It is noteworthy that the effective diffusivity coefficient (D_e) does not significantly varies with the concentration (i.e., D_e: 0.86 ± 0.01 × 10^{-14} m^2 min^{-1}).

The sorbent shows an intermediary behavior among alternative sorbents in terms of apparent rate coefficients; however, under fixed concentrations the equilibrium is reached in about 30 ± 5 min: CTTR is kinetically efficient for Pt(IV) sorption.

3.2.3. *Sorption isotherms and thermodynamics*

The sorption isotherms of Pt(IV) on CTTR are compared for different temperatures in Fig. 5, at pH_0 4. Consistently with Fig. 3, the sorption capacity progressively decreases with increasing the temperature, from 1.58 to 1.19 mmol Pt g^{-1} (at 21 °C and 50 °C, respectively). The binding of Pt(IV) on CTTR is exothermic. The sorption isotherms are characterized by three sections: (a) initial steep increase in sorption capacity, (b) progressive increase (stronger curvature of the plots), and (c) a weak-slope section for approaching the saturation. Table 2 summarizes the parameters for Langmuir, Sips, and Temkin models (whose equations are reported in Table S2b). The Freundlich and the Dubinin-Radushkevich equations were also unsuccessfully tested for fitting experimental profiles (see Table S7, and Fig. S11). The mechanistic Langmuir equation describes a sorption process occurring without interaction between sorbed molecules accumulated as a monolayer at the surface of the sorbent (where the reactive groups bind Pt(IV) with similar sorption energy). The Sips equation is a combination of Langmuir and Freundlich equations, accounting for heterogeneities on the sorbent. The Temkin equation supposes that the sorption energy

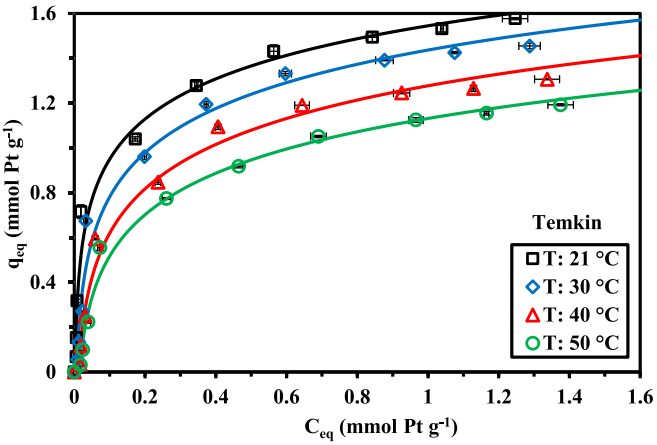

Fig. 5. Pt(IV) sorption isotherms using CTTR at T: 21 °C and 50 °C – Temkin equation fits (C_0: 0.255–1.806 mmol Pt L^{-1}; pH_0: 4; pH_{eq}: 3.82–3.74 at 21 °C increasing to 4.14–4.08 at 50 °C; SD: 0.333 g L^{-1}; v: 220 rpm; time: 48 h).

Table 2
Pt(IV) sorption isotherms – Parameters of the models.

Model	Parameter	Unit	Temperature			
			21 °C	30 °C	40 °C	50 °C
Experimental	$q_{m,exp}$	mmol g^{-1}	1.58	1.45	1.31	1.19
Langmuir	$q_{m,L}$	mmol g^{-1}	1.52	1.51	1.42	1.31
	b_L	L $mmol^{-1}$	27.7	12.3	7.65	6.09
	R^2	–	0.968	0.975	0.984	0.983
	AIC	–	−43	−47	−54	−58
Sips	$q_{eq,S}$	mmol g^{-1}	1.78	1.57	1.37	1.28
	b_S	$(L\ mmol^{-1})^{1/n}$	5.81	8.42	10.2	7.13
	R^2	–	0.975	0.975	0.984	0.983
	AIC	–	−42	−44	−51	−52
Temkin	A_T	L $mmol^{-1}$	392	155	87.1	69.2
	b_T	J kg^{-1} mol^{-2}	9.45	8.86	9.11	10.06
	E_T	kJ mol^{-1}	6.00	6.09	6.97	8.44
	R^2	–	0.984	0.982	0.988	0.991
	AIC	–	−51	−51	−58	−64

decreases with the progressive coverage of sorbent surface. The comparison of the statistical criteria (i.e., R^2 and AIC) in Table 2 shows that the best fit of experimental profiles corresponds to Temkin equation (appearing in Fig. 5 as solid lines), compared with Langmuir and Sips equations (Fig. S12). The Temkin parameter (i.e., A_T) strongly decreases with increasing temperature, from 392 L $mmol^{-1}$ to 69.2 L $mmol^{-1}$. On the opposite hand, the energetic Temkin parameter hardly varies with temperature in the range 8.86–10.06 J kg^{-1} mol^{-2}. The Temkin energy (i.e., $E_T = b_T/q_m$) increases with temperature slightly from 21 to 30 °C (6.00 and 6.09 kJ mol^{-1}, respectively) and more significantly at higher temperatures (6.97 and 8.44 kJ mol^{-1} for 40 and 50 °C, respectively). Though the Langmuir Dual Site equation does not statistically fit experimental profile as fine as the Temkin equation (Fig. S12), this model is interesting because it considers metal sorption on a sorbent bearing two types of reactive groups (individually adopting the Langmuir rules) with different affinity and energy for the sorbate. This model accounts for the duality of the functional groups present on CTTR: N-based and S-based reactive groups. Based on LDS simulation one of the groups shows a much stronger contribution to Pt(IV) uptake (as shown by the highest values of both $q_{m,1}$ and b_1). The affinity coefficient (b_1) of these groups significantly decreases with the increase in temperature. In the figure annexed to Table S7, the contribution (in percentage) of Site 1 (the stronger reactive groups) is calculated (with reference to total sorption). With increasing Pt(IV) concentration, the Site 2 contributes more significantly to total sorption; however, this contribution decreases with increasing the temperature. Pearson [37] established that

soft acids (including Pt(IV)) react preferentially with soft bases (including S-based groups; while N-based ligands are considered hard bases). Tentatively, it is possible suggesting that N-bearing groups having lower affinity for Pt(IV) require high metal concentration for contributing significantly to platinum removal; however, this contribution is very sensitive to temperature (lower affinity at high temperature).

The thermodynamic parameters were determined using the van't Hoff equation, adopting the concept described by Tran et al. [66], with the Langmuir parameter (for the calculation of equilibrium constant, K_e based on b_L, expressed in L mol^{-1}).

$$K_e = b_L \times \frac{C^0_{sorbate}}{\gamma_{sorbate}} \tag{1a}$$

where $C^\circ_{sorbate}$ is the unitary standard concentration of the sorbate (~1 mol L^{-1}) and $\gamma_{sorbate}$ is the activity coefficient (dimensionless).

$$lnK_e = \frac{-\Delta H^\circ}{R} \times \frac{1}{T} + \frac{\Delta S^\circ}{R} \tag{1b}$$

$$\Delta G^\circ = \Delta H^\circ - T\Delta S^\circ \tag{1c}$$

ΔH° (kJ mol^{-1}) is the enthalpy change, ΔG° (kJ mol^{-1}) is the standard change in Gibbs free energy, and ΔS° (J mol^{-1} K^{-1}) is the standard entropy change (R, the universal gas constant, J mol^{-1} K^{-1}).

Fig. S13 shows the van't Hoff plots. The Langmuir equation fits the sorption isotherm with less accuracy than for other temperatures. This may explain the low value of determination coefficient (i.e., 0.938). However, this calculation gives an approximation of thermodynamic parameters (Table S8). The enthalpy changes is close to −17.8 kJ mol^{-1}: the negative value confirms the exothermic nature of Pt(IV) sorption on CTTR. The entropy change reaches −24.1 J mol^{-1} K^{-1}: the negative values indicate that Pt(IV) sorption leads to a decrease of the disorder (randomness) of the system. Despite the negative value of entropy change, the sorption process is spontaneous and exergonic: the standard change of Gibbs free energy is negative and ranges between −10.7 and − 10.0 kJ mol^{-1}. The temperature hardly influences the spontaneity of the sorption. In the case of Pt(IV) sorption on cysteine-functionalized polyurethane foam, Xue et al. [63] reported enthalpy change in the same order of magnitude (i.e., −11.86 kJ mol^{-1}) with lower entropy change (i.e., −12.44 J mol^{-1} K^{-1}), and lower Gibbs free energy change (i.e., decreasing (in absolute value) from −8.16 to −7.60 kJ mol-1 in the range 25–70 °C). In the case of another sulfur-based sorbent (i.e., 3-mercaptoproprionic acid functionalized Fe_3O_4), the enthalpy change reached up to −50 kJ mol^{-1} (with entropy change up to −61 J mol^{-1} K^{-1}) [67].

The sorption isotherms collected at different temperatures can also be used for the determination of the apparent isosteric heat of adsorption ($\Delta H_{is,a}$, kJ mol^{-1}) using the Clausius-Clapeyron Eq. (2) [68]. The equilibrium concentrations (C_{eq}, mmol Pt L^{-1}) reached at different temperatures for different loadings of the sorbent (herein q_{eq}: 0.15, 0.3, 0.45, 0.6, 0.8, 1 and 1.15 mmol Pt g^{-1}) can be used in the following equation for drawing the plots derived from Eq. (2a). The value of $\Delta H_{is,a}$ is obtained from the slope of ln (C_{eq}) vs. the reciprocal of absolute temperature (Eq. (2b)) (Fig. S14a):

$$\frac{d(lnC_{eq})}{dT} = \frac{-\Delta H_{is,a}}{RT^2} \tag{2a}$$

$$ln(C_{eq}) = \frac{\Delta H_{is,a}}{RT} + Cst. \tag{2b}$$

The values of C_{eq} were extrapolated from Temkin best fits. The plots of ln C_{eq} vs. 1/T give linear trends: the linearity of fits is enhanced with surface coverage (from 0.947 to 1.000). The apparent isosteric heat of adsorption varies around −45.0 ± 1.1 kJ mol^{-1} (Fig. S14b). This is consistent with the negative value of the enthalpy change (exothermic reaction). The isosteric heat of Cu(II) sorption on anionic starch beads was negative [69]. Saeed et al. [70] also reported negative ΔH_{is} values for dye sorption on chitosan/MOF composite, while As(III) removal using Zr(IV)/2-thiobarbituric polymer gel was characterized by positive value of ΔH_{is} [68].

Actually, the true isosteric heat of adsorption $\Delta H_{is,net}$ may be deduced from Eq. (3a) [71,72]:

$$\Delta H_{is,a} = \Delta H_{is,net} - \Delta H_{sol} - f\Delta H_w \tag{3a}$$

where f is the number of water molecules exchanged during sorption, since ΔH_w (the heat of adsorption of water) is usually considered negligible, Eq. (3a) can be simplified to Eq. (3b):

$$\Delta H_{is,a} \approx \Delta H_{is,net} - \Delta H_{sol} \tag{3b}$$

where ΔH_{sol} is the heat of solution for $PtCl_4$ (i.e., 82.0 kJ mol^{-1}). Therefore, $\Delta H_{is,net}$ is close to +37 kJ mol^{-1}.

The variation of the isosteric heat of adsorption with the increase of sorbate loading is generally correlated with the occurrence of lateral interactions between adsorbed sorbate molecules [71]. Herein, the change in the isosteric heat of sorption is almost negligible. It is thus consistent with the condition requested for application of Langmuir equation (no interaction between sorbed molecules).

Table S9 reports the sorption performances of CTTR in comparison with those of alternate sorbents. The criteria consider the preferred pH or acid concentration, the equilibrium time under selected experimental conditions, the maximum sorption capacity both experimental and calculated by the Langmuir equation, and the Langmuir affinity coefficient. The strict comparison is made difficult by the differences of experimental conditions (pH as mentioned and other parameters such as the sorbent dose for kinetic evaluation). Some sorbents show remarkable sorption capacities such as graphene oxide/dendritic (aminated) sorbent (4.2 mmol Pt g^{-1}) [60], PEI/S functionalized POSS dendritic sorbent (2.43 mmol Pt g^{-1}) [1], PEI functionalized PE/PP non-woven fabrics (2.49 mmol Pt g^{-1}) [61], diethylthiocarbamate cellulose (DTC-Cellulose, 2.01 mmol Pt g^{-1}), PEI-PVC fibers (2.00 mmol Pt g^{-1}) [50]. These sorption levels exceed the maximum sorption capacity of CTTR (1.58 mmol Pt g^{-1}); however, the fast uptake kinetics (equilibrium time 40 min compared with 70 min to 144 h contact times) partially compensates this limitation. The affinity coefficient (27.7 L mmol^{-1}) is relatively high compared to these materials (except for DTC-Cellulose, where b_L reached up to 74.4 L mmol^{-1}). These comparative data confirm the interest for the recovery of Pt(IV) from weakly acidic solutions. Other sorption figures may be considered for comparing and selecting the sorbent: the capacity to re-use the sorbent and the selectivity of the sorbent for platinum (see below).

3.2.4. Sorption mechanism

Optimum sorption occurs at a pH value lower than the pH_{pzc}. This means that the sorption of platinum is favored under conditions where the surface of the sorbent is positively (or partially positively) charged. The electronegativity of reactive groups decreases according: O > N > S. These conditions are also favored by the tautomerization effects associated with partial delocalization of charges on N and S moieties. FTIR spectra confirm the formation of secondary amine (the tautomerization is supported by the choice of both heterocyclic monomers and cross-linker). The XPS analysis provides data parallel to the FTIR spectra and clarifies the interaction of CTTR with metal ions. The quaternary amine groups bring anion exchange properties for selective interaction with Pt anion species ($HPtCl_6^-$, $PtCl_6^{2-}$, $PtCl_5(H_2O)^-$ and $PtCl_4(H_2O)(OH)^-$). It is noteworthy that the changes in XPS spectra of N 1s (in terms of both BEs and AFs for QA groups) confirm the direct interaction with Pt anionic species. The tertiary amine (also confirmed in HRES spectra) shows high performance for metal binding as well as good contributor for the reduction of Pt through its electron donor properties. This process was also assisted by thiol groups (resulting from tautomerization mechanisms), which also directly bind Pt ions (but also participate in the

reduction process). The high proportion of Pt(II) (i.e., about 72.5 % of total Pt) confirms that in mild acid conditions (selected for metal sorption), the metal is substantially reduced due to the abundance of groups bearing electron donor atoms. In the study of pH effect, the slope analysis of the plot $\log_{10}$ D vs. pH_{eq} (i.e., 0.94) is consistent with the occurrence of an ion-exchange mechanism. This is also consistent with the predominance of negatively-charged platinum species under these optimum conditions. The combination of these different observations allows proposing the modes of interactions illustrated by Scheme 2. Platinum binding occurs through anion-exchange/electrostatic attraction of negatively-charged platinum chloride species (preferentially $PtCl_3^-$) with quaternary amine groups and/or partially positive groups (driven by electronegativity properties and tautomerization effects). Mild acidic condition and electron donner groups (grafted during synthesis or produced as a result of tautomerization) have a great potential for reducing Pt(IV) to Pt(II). This was confirmed by BE shifts and increases of the AF% for QA, accompanied by the decrease of other amine species (i.e., secondary and tertiary amine peaks). At the meantime the XPS interpretation is consistent with the existence of four deconvoluted peaks (2 spin-orbit doublets for Pt(IV) and Pt(II) forms). Based on the remarkable properties of the sorbent (compared with literature), it appears that the bulky nature of heterocyclic moieties in the sorbent do not introduce steric hindrance (which could have influenced the accessibility to reactive groups and consequently the sorption capacities).

3.2.5. *Metal desorption and sorbent recycling*

Designing a new sorbent requires evaluating the possibility to desorb the sorbent and to recycle the material for the competitiveness of the global process. Another important criterion concerns the capacity to concentrate the sorbate through the combination of sorption/desorption operations. To address these objectives the kinetics of desorption are first compared for three eluents (Fig. 6): (a) HCl (0.3 M, acidic eluent), (b) thiourea (1 M, complexing agent), and (c) sodium perchlorate (strong oxidizing agent). Four different solid/liquid ratio in the eluent solution are tested (i.e., 1.33 to 3.33 g L^{-1}). The eluents can be readily ranked according: 0.3 M HCl >1 M $NaClO_4$ > 1 M thiourea, considering the level of desorption, the maximum sorbent dose admissible for complete Pt(IV) desorption, and the time required for achieving the complete desorption. Thiourea does not reach complete desorption even at the lowest S/L ratio; the efficiency of the complexing agent would probably increase with addition of HCl [73]. The desorption may be affected by the partial reduction of Pt(IV) that makes a fraction of the metal refractory to complexation by thiourea. In the case of sodium perchlorate full desorption is only observed for S/L = 1.33 g L^{-1}, where a contact of 60 min is required. The strong oxidizing agent favors restoration of Pt(IV) for desorption. Hydrochloric acid (at mid concentration: 0.3 M) reveals highly efficient for the release of Pt(IV) from metal-loaded CTTR. Indeed, the full desorption is observed with both S/L: 1.33 and 1.67 g L^{-1}. In addition, with S/L: 1.33 g L^{-1}, 30 min of contact are enough (against 60 min at S/L: 1.67 g L^{-1}). The acidity and the concentration of chloride ions both contribute to the formation of $PtCl_6^{2-}$ highly soluble species, and then to the reversal of metal sorption. The normal redox potential of Pt(IV)/Pt(II) is close to 0.726 V. Hydrochloric acid is not a strong oxidant; however, it is enough oxidizing for processing the dissolution of zinc metal (Zn(II)/Zn(0) has a comparable normal redox potential; i.e., 0.76 V). This double effect may explain the good efficiency of 0.3 M HCl solution for eluting Pt(IV) from CTTR. These results contrast with the conclusions raised by Dobrowolski et al. [56] for Pt(IV) elution from amino-functionalized mesoporous silica: desorption efficiency decreased according thiourea > HNO_3 > HCl. Fayemi et al. [74] recommended thiourea solutions (at 3 % m/v concentration) for recovering PGMs from polyamine-functionalized polystyrene. However, they suggested a sequential treatment for the selective separation of Pt(IV) from Pd(II) using first 0.5 M $NaClO_4$/1 M HCl and then 0.5 M thiourea/1 M HCl. Acidic thiourea solutions were preferred for the elution of PGMs from a series of commercial resins [75], and from graphene oxide dendritic adsorbent [60]. In the case of PEI-functionalized PVC fibers, Bediako et al. [50] reported the quantitative desorption of Pt(IV) with 0.1 M thiourea solution. The desorption step can be used to complete the selective separation when the sorption step is not enough: for example, in the treatment of leachates (of spent reforming catalysts), the ion exchange resin (DiaionSA10AP) bound both platinum and iron. Iron was eluted with dilute HCl solution (0.0001 M), while platinum was recovered with 0.1 M thiourea solution

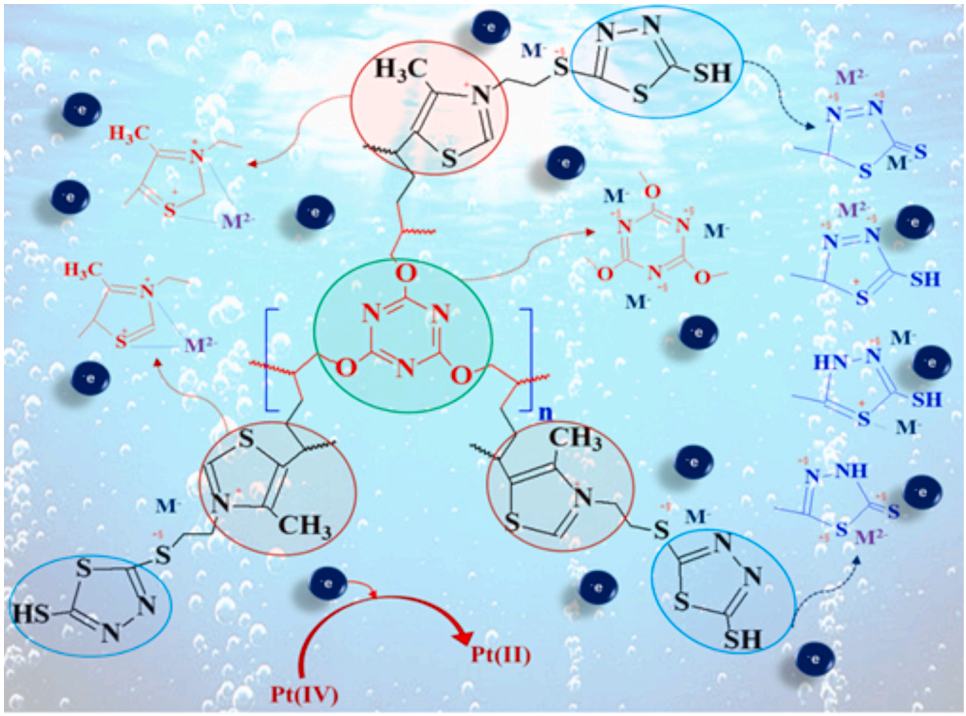

Scheme 2. Suggested mechanisms of Pt(IV) sorption on CTTR

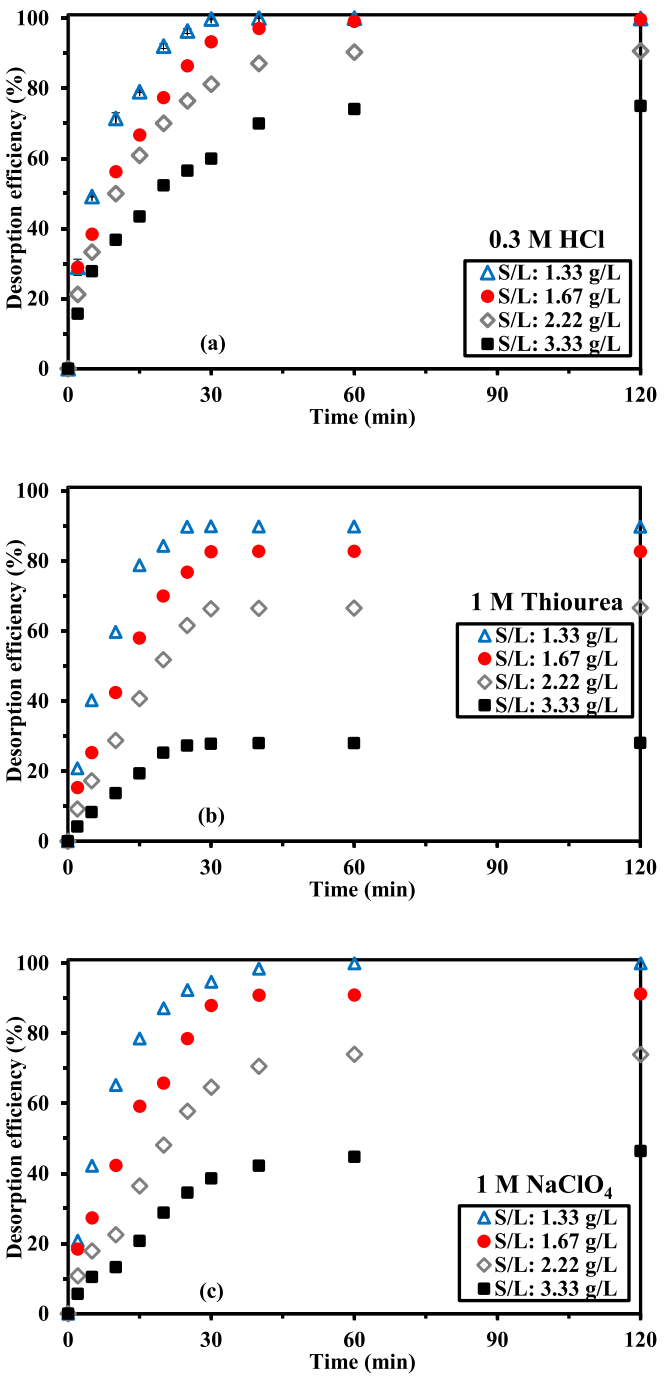

Fig. 6. Comparison of Pt(IV) desorption performances using 0.3 M HCl, 1 M thiourea and 1 M $NaClO_4$ solutions at different S/L (solid/liquid) ratio (Pt-loaded sorbent collected from the study of sorption kinetics; for desorption step: v: 220 rpm; T: 21 ± 1 °C).

[76].

In Fig. S15, the effect of S/L ratio on Pt(IV) release is examined under the double criterion of sorption efficiency (at 480 min of contact) and enrichment factor (meaning the ratio of Pt concentration in the eluate vs. the initial concentration in the loading solution). Logically, increasing the S/L ratio decreases the efficiency of the elution but increases the enrichment factor. Due to the high commercial value of platinum, the main objective remains the full recovery of the sorbent: herein, the optimized conditions correspond to S/L ratio close to 1.67 g L^{-1}; however, the enrichment factor cannot exceed 4.6.

A complementary experiment illustrated by Fig. S16 shows that increasing the temperature in the elution steps does not change the efficiency of the desorption (which is total under selected experimental conditions) but significantly increases the desorption kinetics: 20 min of contact are enough at T: 50 °C for achieving the complete desorption (vs. 30 min at 21 °C). This result is consistent with the thermodynamic characteristics of Pt(IV) removal: spontaneous and exothermic sorption. Therefore, increased temperature favors the reversal of metal binding.

To complete this overview of desorption properties, the capacity of the sorbent to be re-used for a series of 5 cycles is illustrated in Table 3. The desorption remains complete over the 5 cycles: platinum does not accumulate at the surface of the sorbent. The sorption efficiency progressively decreases at re-use. However, even at the fifth cycle, the loss in sorption performance does not exceed 3.5 %. The re-use of PEI-PVC sorbent also revealed a progressive loss in sorption performance with 0.1 M thiourea eluent (of the same order of magnitude of current work) [50]. At the third cycle, the loss in Pt sorption represented about 3 % while using dendritic graphene oxide sorbent with acidic thiourea solution. On the opposite hand, in the case of PEI-loaded chitosan hollow beads, the desorption of Pt(IV) with 0.1 M thiourea solution leaded to significant loss in sorption stability (from 97 % to 46 %) [77]. Apparently, CTTR is part of the most efficient sorbents considering the stability of sorption performances at recycling, as another proof of the promising performances of this material.

3.2.6. *Sorption selectivity*

The selectivity in sorption is another important criterion that must be considered when designing a new sorbent. To assess the potential of CTTR to selectively recover Pt from complex solutions, a first study carried out metal sorption tests at different pH values (in the range pH_0: 1.02–3.98) using equimolar multicomponent solutions (C_0: 0.2 mmol L^{-1}). Selected competitor metals have been selected for their physico-chemical characteristics (ionic charge, soft/hard character according the Pearson's principles, and their possible presence together with platinum). The sorption capacities, the distribution ratios, and the selectivity coefficients ($SC_{Pt/Metal}$) are successively presented in Fig. 7.

$$SC_{Pt/Metal} = \frac{D_{Pt}}{D_{Metal}} = \frac{\left(q_{eq.Pt}\right) \times \left(C_{eq.Metal}\right)}{\left(C_{eq.Pt}\right) \times \left(q_{eq.Metal}\right)} \quad (4)$$

Increasing the pH systematically increases the sorption of the metal ions because of the decreased competition of protons and the enhancement of chelation properties at mild pH. Hence, the cumulative sorption capacity increases from 0.156 mmol g^{-1} at pH_{eq} 1.15 to 1.11 mmol g^{-1} at pH_{eq} 3.84. This cumulative sorption capacity is in equilibrium with a total residual concentration of 0.93 mmol g^{-1}. Under similar residual concentration, the sorption capacity for single-component solution at 21 °C reached 1.51 mmol Pt g^{-1}. This means that the competitor metal ions have an antagonist effect on Pt(IV) sorption [78]: the metal ions compete (at least partially) for the same reactive groups. Pd(II) and Pt (IV) roughly follow the same trends with comparable sorption capacities, significantly higher (up to 0.26 mmol g^{-1}) than those obtained for other competitor ions (in the range 0.07–0.16 mmol g^{-1}, for the other metal ions at pH_{eq} 3.84). It is noteworthy that these metal ions have

Table 3
Recycling of CTTR - Pt(IV) sorption (SE) and desorption (DE) efficiencies (%).

Cycle	SE (%)		DE (%)	
	Aver.	Std. Dev.	Aver.	Std. Dev.
#1	97.00	1.26	100.06	0.05
#2	96.06	1.21	100.05	0.07
#3	95.07	1.55	100.41	0.10
#4	94.61	1.38	100.08	0.01
#5	93.62	1.85	100.07	0.09
Loss at 5th cycle*	3.48		Negligible	

* Compared with initial cycle.

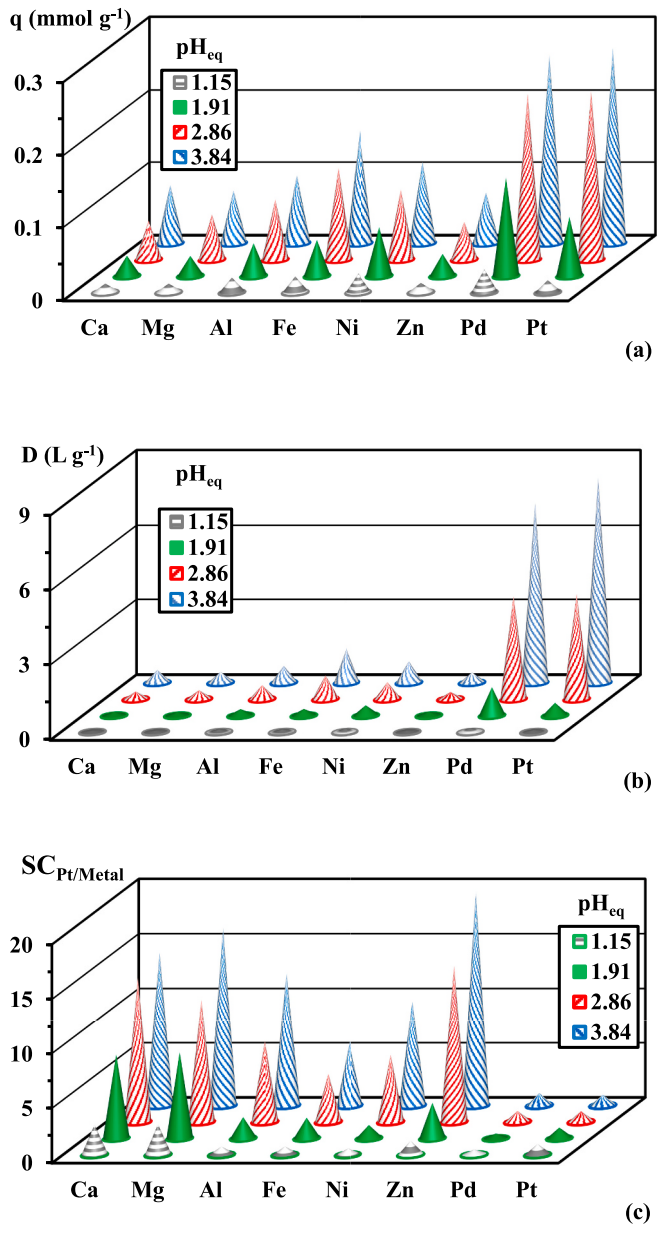

Fig. 7. Metal sorption from multi-metal equimolar solutions using CTTR at different pH values – (a) sorption capacity, q (mmol g^{-1}), (b) Distribution ratio, D (L g^{-1}), and (c) selectivity coefficient, $SC_{Pt/metal}$ (C_0: ≈0.2 mmol L^{-1}; pH_0: 1.02–1.99-3.02-3.98; SD: 0.666 g L^{-1}; T: 21 ± 1 °C; time: 24 h; $SC_{Pt/Pt}$ = 1 as reference).

strong affinity for chloride ligands to form chloroanionic complexes in acidic conditions, contrary to the other metal ions included in the panel. They are both member of the Class-B (soft metals) according the Pearson's classification [37]. CTTR holds both S-based and N-based reactive groups. Pearson reported the order of stability of soft metals ions with ligands bearing the following donor atoms, according to: S > Cl > N > O. Soft acids prefer to associate with soft bases. Hard acids (such as Ca(II), Mg(II), and Al(III)) are supposed to follow a reciprocal trend in terms of affinity for the reported ligands. This is consistent with the lower sorption capacities observed for Ca(II), Mg(II), and Al(III) (below 0.095 mmol g^{-1}). The other metal ions (i.e., Fe(III), Ni(II), and Zn(II)) are classified among borderline (intermediary) metals [38]; they show intermediary sorption figures: Fe(III) (0.156 mmol g^{-1}) > Ni(II) > Zn(II) (0.070 mmol g^{-1}). This ranking is consistent with the decrease in their class B character. It is noteworthy that Pearson [37] also classified Fe (III) among hard metals.

Fig. 7b highlights the differences between the plots of metal distribution ratios at the different pH values. Platinum and palladium show remarkable values that can reach in mild acidic solutions (i.e., pH_{eq} 3.84) up to 8.2 and 7.2 L g^{-1}, respectively; while for other metal ions the $D_{pH3.84}$ values range between 0.42 and 1.40 L g^{-1}. The metal ions can be ranked according:

Pt(IV) > Pd(II) >> Fe(III) > Ni(II) > Al(III) > Ca(II) > Mg(II) > Zn(II).

In Fig. S17, the D values and the q values are plotted against the softness parameter σ [65]. The plot of sorption capacity shows relatively good "linear" correlation between q and σ, with the remarkable exception of Zn (for which sorption capacity is much lower than expected from linear trend). The plot of the distribution ratio vs. σ follows an exponential trend (with again marked discrepancy of zinc). It is noteworthy that zinc also "escapes" the Irving-Williams series; in the divalent cations series, zinc exhibits a "zero crystal field stabilization energy" (CFSE), while in the divalent first-row transition family, the CFSE increases from manganese to nickel. The Irving-Williams series is frequently associated with the relative facility of aqua ligand to be exchanged with the other ligand in the metal complex. In Fig. S18, the D and q values are plotted against the enthalpy of hydration of the different metal ions [79]. The metal ions can be grouped in three blocks: (a) low (absolute) value of the hydration enthalpy (around 740 kJ mol^{-1}) for PGMs, (b) medium $-\Delta H_{hydr.}$ values (i.e., 1600–2120 kJ mol^{-1}) for divalent metal cations, and high $-\Delta H_{hydr.}$ values (4460–4720 kJ mol^{-1}) for trivalent metals ions. There is not direct correlation between hydration enthalpy and the affinity of the sorbent for selected metals except that PGMs have much lower enthalpies and strong affinity for CTTR. The ligand exchange may be mediated by the chloro-complexes of Pd and Pt. Apart the complexation of metal ions, the ion-exchange mechanism (which is favored by the predominance of chloroanionic species) also contributes to favoring their binding against other competitor metal cations.

3.3. *Recovery of platinum from solid waste*

The catalysts that do not comply with the commercial specifications are discarded. Herein, the Pt catalysts were based on alumina support and contain also titanium (at very low percentage, Table S10). Fig. S19 shows the X-ray diffractogram (XRD) of the catalyst sample. Most of the peaks can be used to identify Al_2O_3 forms (γ-Al_2O_3 as boehmite and η-Al_2O_3 as bayerite) [80,81]; however, some unexpected peaks can also be observed at 2θ: 18.50° and 20.32°. In conventional Al_2O_3 solids, the (111) reflection should appear at 2θ: ≈19.56° as a single peak more (η-) or less (γ-) resolved [80]. This doublet appears on the XRD pattern of Al $(OH)_3$ [82]. The broad peak at 2θ: 27.86° may also correspond to contributions of aluminum hydroxide [82]. The Ti content is too weak (i.e., Ti traces: 0.00055 %) to be detected in the XRD. The semi-quantitative EDX analysis shows the significant presence of carbon (up to 3.69 mass %, 5.80 mol%), as contaminant traces. The presence of Pt coating is characterized by the peaks at 2θ: 39.39° (Pt (111)) and 85.15° (Pt (311)); a third one was reported at 2θ: ≈46.3° (Pt (200)) by Silva Júnior et al. [83], but here it is probably superposed to the 2θ: 46.04° peak of alumina phase. It is noteworthy that the molar ratio Al/Pt in the catalyst exceeds 411 (based on the percentage of metals in the solid, Table S10).

Table S10 shows the mass percentage of the metals in the non-compliant catalyst. Platinum content does not exceed 0.57 % (in mass); meaning that aluminum (at ≈32.6 %) is in large excess (while titanium is just present at trace level). The recovery of PGMs from spent catalyst-based materials consists of leaching processes [18,84,85], eventually combined with roasting in the case of carbon-poisoned spent catalysts [86], or acidic fusion [16,87]. Though alkaline processes (such as cyanidation) have been used for platinum recovery from PGM resources [24]; in most cases acidic solutions are preferred including organic acids [88], inorganic acids [14,89] (with addition of H_2O_2,

[15]). Aqua regia giving both acidic and oxidizing conditions is also frequently used [13,18,90]. Based on the high efficiency, the absence of organic poisoning, and the acidic oxidizing nature of aqua regia, this leaching agent was selected for the treatment of non-compliant Pt/Al_2O_3 catalyst.

3.3.1. Leachate

Table S10 also shows that the process is highly efficient for leaching platinum (about 97 % yield), with simultaneous release of titanium traces (at ≈91 %). Unfortunately, aluminum is also leached; though the yield is limited to 25.3 %, the concentration of Al in the leachate reaches about 30 g Al L^{-1}. This is much higher than Pt concentration (about 2.02 g Pt L^{-1}); with negligible amount of titanium (i.e., 1.8 mg Ti L^{-1}). These contents are obviously consistent with the percentage of the three metals in the catalyst; though the leaching allows reducing the molar ratio Al/Pt (in the leachate) to 107.5. The concentration of Pt is not appropriate for direct sorption; the concentrating effect of sorption/desorption would not be competitive enough compared with solvent process; concentrations around or below 200 mg L^{-1} are more appropriate. In addition, the presence of huge concentrations of aluminum would have a strong competition effect on sorption properties. For these reasons, pre-treatments are necessary before processing sorption tests. Ammonium chloride is well known for use as platinum precipitant with relative selectivity against other PGMs, but also other metals present in the leachates of catalysts [17,21,22]. Table S10 shows the residual concentrations of the metals after NH_4Cl precipitation: platinum is recovered with a yield that reached 92.5 %, while the residual concentration decreases to 151 mg Pt L^{-1} (which would be consistent for sorption operations). Aluminum is also partially precipitated (by 27.5 %); residual concentration remains as high as 21.7 g Al L^{-1}. This means that the molar ratio Al/Pt in the pre-treated leachate reaches about 1040. Despite the large preference of CTTR for Pt(IV) against Al(III) (Fig. 7), this large excess will introduce constraints and competition in Pt (IV) sorption. The second pre-treatment is processed using NaOH for controlling the pH of the solution to 5 by Al precipitation (as $Al(OH)_3$). Table S10 confirms the efficiency of this treatment in the reduction of residual Al concentration to 188 mg Al L^{-1} (precipitation exceeds 99 %), leaving platinum concentration close to 98 mg Pt L^{-1}. The final molar ratio Al/Pt strongly decreases to 13.9: under these conditions (lower excess of competitor ion, and concentration values), the sorption process is applicable. Fig. S20 shows the distribution of the metals in the different compartments (NH_4Cl precipitate, NaOH, and working sorption solution) involved in the pre-treatment of leachates. Platinum is essentially present in the selective NH_4Cl precipitate (≈92.5 %); ≈2.6 % is co-precipitated at pH 5. Aluminum is mainly collected in the NaOH precipitate (≈71.8 %), with a significant part (≈27.5 %) being present in the NH_4Cl precipitate. Titanium traces are present in the three compartments (≈50.8 % in NH_4Cl precipitate, ≈22.7 % in NaOH precipitate). The mass balance data for the different steps of the pre-treatment process are also reported in this figure.

3.3.2. Sorption

Fig. 8 compares the sorption and separation of the three metals from pre-treated leachate at different pH values using CTTR. The sorption of titanium is negligible (due to the large excess of other metal ions in the leachate compared with Ti(IV)). For aluminum, the sorption capacity progressively increases with the pH up to 4 (from 0.076 to 0.63 mmol Al g^{-1}), before tending to stabilize (at pH 5: q_{eq} tends to 0.67 mmol Al g^{-1}) (Fig. 8a). In the case of Pt(IV), the sorption capacity increases from 0.023 to 0.049 mmol Pt g^{-1}, when the pH is shifted from 1 to 2, and the sorption capacity hardly increases above pH 2. This gives a first indication for the selection of preferential pH value for optimized separation of Pt(IV) from Al(III). In Fig. 8b, the plot of the distribution ratios shows

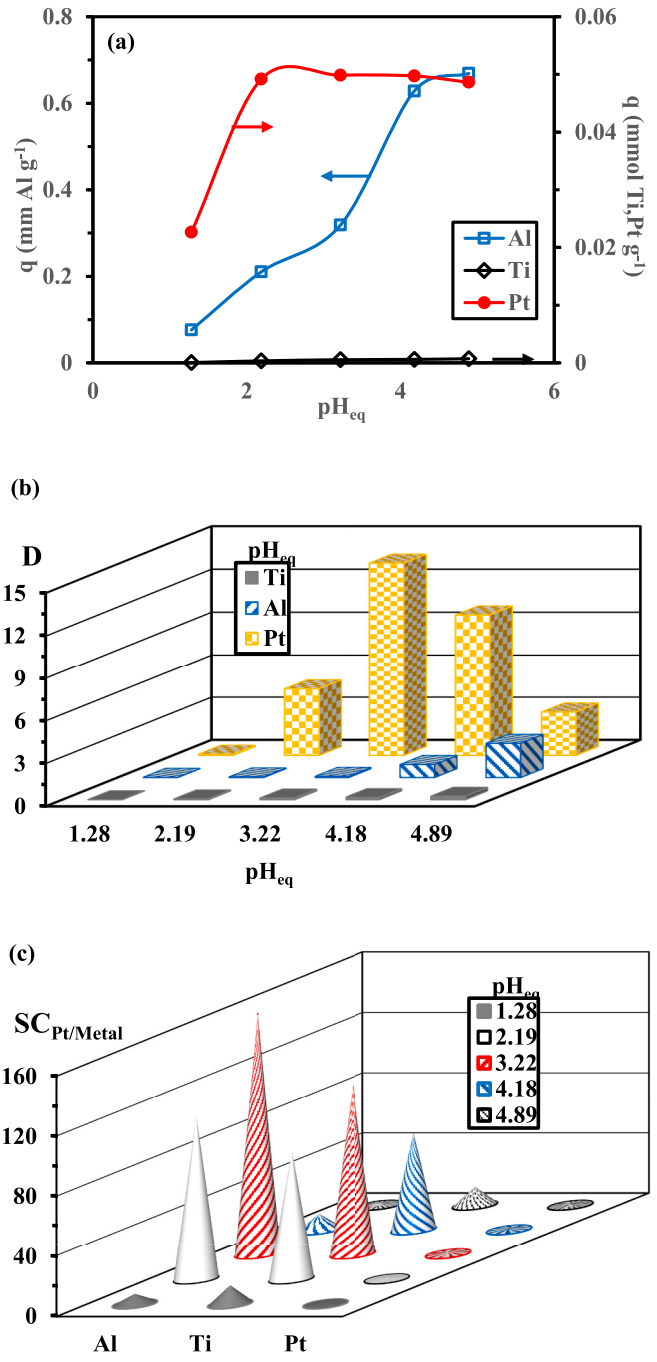

Fig. 8. Metal sorption for pre-treated leachates of catalyst waste: (a) sorption capacity, (b) distribution ratio, and (c) $SC_{Pt/metal}$ (pH_0: 1.02–2.01-3.01-4.02-5.01; SD: 10 g L^{-1}; T: 21 °C; time: 60 min).

a clear maximum (up to 13.5 L g^{-1}) for Pt(IV) at pH_{eq} 3.22, while for Al (III), the D value does not exceed 0.085 L g^{-1}. With increasing the pH_0 above 3, D(Pt) progressively decreases, while D(Al) increases. The selectivity coefficient $SC_{Pt/metal}$ offers another visualization of the differences in sorption performances; and Fig. 8c clearly shows that the best separation is achieved at pH_{eq} 3.22: up to 160.6 against Al(III) and 144.3 against Ti(IV). The sorption yield reaches at this pH up to 99.3 % for Pt(IV) against 54.2 % for Ti(IV), and 45.7 % for Al(III). Aluminum and titanium are members of the hard acids, contrary to platinum soft acid. According the hard and soft acid and base theory [37], S-based

ligands (soft bases) preferentially react with soft acids. Therefore, the selectivity of CTTR for Pt(IV) against Al(III) and Ti(IV) is consistent with this principle. This is also supported by the differences in their chemistry in solution and the formation of chloroanionic platinate species that can bind to protonated amine groups under these experimental conditions.

Based on the results reported in Figs. S22a-c, the cost associated with full Pt(IV) recovery (i.e., sorption yield $\geq$99 %) can be compared for the three sorbents:

$$\text{Lewatit®MonoPlus TP214 } (38.5 \text{ USD}) < \text{CTTR } (87.2 \text{ USD}) < \text{Dowex } 1 \times 8 \ (107,0 \text{ USD}).$$

Fig. S21 shows the general flowsheet for the treatment of non-compliant catalysts and the global data for treatment efficiency at the different steps. Semi-quantitative EDX analyses of the precipitates are also reported. The leaching of platinum is highly efficient (yield is close to 97 %), contrary to Al (about 25 %). The precipitation of platinum as ammonium salt using ammonium chloride is effective (reaching 92.5 %). The semi-quantitative EDX analysis of platinum precipitate shows the presence of traces of aluminum (2.45 %, in weight). The residual platinum concentration in the filtrate is close to 151 mg Pt L^{-1} (with a huge excess of aluminum, at the concentration of 21.7 g Al L^{-1}). When the sorption is directly processed on the filtrate (of $Al(OH)_3$ precipitation) it is necessary working at pH close to 3.2 to quantitatively remove platinum (partly due to co-precipitation with aluminum hydroxide). The pre-treatment by pH control at 5 allows removing quantitatively aluminum with a loss of Pt(IV) limited to 35 %: Pt content in aluminum hydroxide precipitate is less than 0.57 %. The pre-treatment produces a filtrate with a Pt concentration close to 98 mg Pt L^{-1}, which is quantitatively recovered by sorption at pH 2.19.

Under comparable experimental conditions, CTTR sorbent allows the full recovery (>96 %) on a wide range of initial pH values (pH 2–5), while for commercial resins the removal of Pt reaches a maximum at pH_0 3 with maximum uptake limited to 28 % for Lewatit® MonoPlus TP214 and down to 15 % for Dowex 1-X8 (Figs. S22a-c). The sorption of Al(III) and Ti(IV) increases with pH for CTTR, while their recovery with commercial resins tends to stabilize in the range pH_0 3–5. To reach a higher selectivity for platinum recovery using CTTR, it may be probably more interesting working at pH_0 2–3; this pH range allows combining high sorption yield and moderate sorption of other metals.

The comparison of sorption properties brings additional information on the interesting performances of CTTR. Hence, Fig. S22d-f, clearly shows that the distribution ratio for Pt is considerably increased at the optimum pH_0 (i.e., 3): $\log_{10}$ D values reaches 1.13 for CTTR (against -1.55 for Dowex 1-X8 and -1.41 for Lewatit® MonoPlus TP214; i.e., 2/3 orders of magnitude lower). On the opposite hand, the commercial resins show higher concentrating effect for the removal of Ti(IV) and Al(III), than CTTR. At pH_0 3, the distribution ratios are reversed between CTTR and commercial resins:

$$\text{CTTR} : \text{Pt} >> \text{Ti} \approx \text{Al}$$

$$\text{Dowex } 1-\text{X8 and Lewatit®MonoPlus TP214} : \text{Al} >> \text{Ti} >> \text{Pt}.$$

It is thus possible anticipating that CTTR provides more interesting separation properties. This is confirmed by the comparison of $SC_{Pt:Metal}$ (Fig. S23): At pH_0 3, CTTR exhibits high selectivity for Pt(IV) over Ti(IV) (up to 114) and Al(III) (up to 161). On the opposite hand, the $SC_{Pt/Metal}$ values are lower than 0.6 in most cases; indicating that the resins have a higher relative efficiency for the removal of Ti(IV) and Al(III). The unique exception concerns Ti(IV) recovery under the most acidic conditions (i.e., pH_0 1) where $SC_{Pt/Ti}$ values vary between 1 and 1.1.4 for the resins (weak preference for Pt(IV)).

CTTR sorbent not only offers higher recovery efficiency for Pt(IV) against the two resins but also provides higher selectivity, which a significant advantage for separation of this precious metal from co-metal ions.

This comparison of costs is based on rough evaluation of the reagents' costs involved in the synthesis of CTTR and the commercial catalogue costs for synthetic resins (see Supplementary Information).

4. Conclusion

The successful synthesis of a sorbent (CTTR) bearing both N- and S-bearing reactive groups (through the quaternization of 4-methyl-5-vinylthiazole with triallyl cyanurate, mediated by AIBN) allows producing a sorbent highly efficient for platinum recovery from aqueous solutions at pH 4. Chloro-anionic platinum species are bound onto protonated amine groups and S-bearing groups (through ion-exchange mechanism, facilitated by tautomerization effects associated with reactive groups in acidic solution). The sorption is exothermic as shown by the comparison of isotherms at different temperatures, which are preferentially fitted by the Temkin equation. Under selected experimental conditions, the equilibrium is reached in 30 min (the kinetic profiles being modeled using the pseudo-first order rate equation). Hydrochloric acid (0.3 M) reveals highly efficient for quantitative desorption of adsorbed platinum, with limited loss at recycling (less than 3.5 % at the fifth cycle), and optimum enrichment factor (i.e., 8) observed at solid/liquid ratio 1.67 g L^{-1}. Tested in multicomponent equimolar solutions, metal sorption (as distribution ratio) can be correlated to the softness of metal ions with a marked preference for Pt (IV) and Pd(II); this effect is reinforced by the effect of pH on metal speciation (formation of anionic species). The sorbent is also successfully applied to recover platinum from non-compliant catalyst beads through leaching and pre-treatment (at pH 5, to reduce the competition effect induced by the huge excess of aluminum, which was co-extracted from the catalyst). Under selected experimental conditions, the sorbent quantitatively recovers platinum at pH 2.2 with limited co-extraction of titanium and aluminum.

The objective of this work consisted in verifying the potential of the bi-functional material for platinum recovery. This preliminary study confirms the potential of CTTR for the removal of PGMs from mild acidic and complex solutions. However, CTTR was designed as micron-size particles; this conditioning allows demonstrating the potential of the material for target objectives. For real-life use, the small size of CTTR particles precludes application in fixed-bed columns (the most appropriate operating mode for dynamic treatment) due to head loss pressure and clogging effect, or continuously-stirred tank reactor (because of complexity in solid/liquid separation). Therefore, after proving the efficiency of the sorbent, the next step for future large-scale application would require investigating agglomeration, entrapment in porous matrix, and/or spherization processes to facilitate the management of sorbent (with a careful attention to the diffusional constraints that may be introduced in the conditioning of the material).

CRediT authorship contribution statement

Mohammed F. Hamza: Writing – review & editing, Visualization, Software, Conceptualization. **Eric Guibal:** Writing – review & editing, Writing – original draft, Software, Investigation. **Yuezhou Wei:** Funding acquisition, Formal analysis, Data curation. **Shunyan Ning:** Resources,

Methodology, Funding acquisition. **Xiangbiao Yin:** Resources, Methodology, Formal analysis. **Amr Fouda:** Investigation, Data curation. **Hamada H. Amer:** Project administration, Funding acquisition. **Saly R. El Dakkony:** Data curation, Conceptualization.

Declaration of competing interest

The authors declare that they have no known competing financial interests or personal relationships that could have appeared to influence the work reported in this paper.

Data availability

Data will be made available on request.

Acknowledgements

National Natural Science Foundation of China [22350710186, U23B20167, 22066005, U1967218, 11975082, and 22206073], the Science and Technology Innovation Program of Hunan Province [2023RC1067], and the Scientific Research Program of FuRong Laboratory [grant number 2023SK2098]. The authors would like to acknowledge Deanship of Graduate Studies and Scientific Research at Taif University for funding this work.

Appendix A. Supplementary data

Supplementary data to this article can be found online at https://doi.org/10.1016/j.susmat.2024.e01165.

References

[1] H. Chaudhuri, C.-R. Lim, Y.-S. Yun, Polyethylenimine functionalized sulfur-containing POSS-based dendritic adsorbent for highly efficient and selective capturing of precious metal ions, Desalination 566 (2023) 116925, https://doi.org/10.1016/j.desal.2023.116925.

[2] C. Hagelüken, D. Goldmann, Recycling and circular economy—towards a closed loop for metals in emerging clean technologies, Miner. Econ. 35 (2022) 539–562, https://doi.org/10.1007/s13563-022-00319-1.

[3] O. Artiushenko, R.F. da Silva, V. Zaitsev, Recent advances in functional materials for rare earth recovery: a review, Sustain. Mater. Technol. 37 (2023) e00681, https://doi.org/10.1016/j.susmat.2023.e00681.

[4] M.S. Safarzadeh, M. Horton, A.D. Van Rythoven, Review of recovery of platinum group metals from copper leach residues and other resources, Miner. Process. Extr. Metall. Rev. 39 (2018) 1–17, https://doi.org/10.1080/08827508.2017.1323745.

[5] F. Nkinahamira, A. Alsbaiee, Q.T. Zeng, Y. Li, Y.Q. Zhang, M.L. Feng, C.P. Yu, Q. Sun, Selective and fast recovery of rare earth elements from industrial wastewater by porous β-cyclodextrin and magnetic β-cyclodextrin polymers, Water Res. 181 (2020) 115857, https://doi.org/10.1016/j.watres.2020.115857.

[6] H.G. Dong, J.C. Zhao, J.L. Chen, Y.D. Wu, B.J. Li, Recovery of platinum group metals from spent catalysts: a review, Int. J. Miner. Process. 145 (2015) 108–113, https://doi.org/10.1016/j.minpro.2015.06.009.

[7] L. Xolo, P. Moleko-Boyce, H. Makelane, N. Faleni, Z.R. Tshentu, Status of recovery of strategic metals from spent secondary products, Minerals 11 (2021) 673, https://doi.org/10.3390/min11070673.

[8] M.Q. Jia, G.S. Jiang, H.C. Chen, Y. Pang, F. Yuan, Z. Zhang, N.Q. Miao, C.Z. Zheng, J.H. Song, Y.Y. Li, et al., Recent developments on processes for recovery of rhodium metal from spent catalysts, Catalysts 12 (2022) 1415, https://doi.org/10.3390/catal12111415.

[9] A. Pathak, H. Al-Sheeha, R. Navvamani, R. Kothari, M. Marafi, M.S. Rana, Recycling of platinum group metals from exhausted petroleum and automobile catalysts using bioleaching approach: a critical review on potential, challenges, and outlook, Rev. Environ. Sci. Biotechnol. 21 (2022) 1035–1059, https://doi.org/10.1007/s11157-022-09636-x.

[10] C. Saguru, S. Ndlovu, D. Moropeng, A review of recent studies into hydrometallurgical methods for recovering PGMs from used catalytic converters, Hydrometallurgy 182 (2018) 44–56, https://doi.org/10.1016/j.hydromet.2018.10.012.

[11] P. Sinisalo, M. Lundstrom, Refining approaches in the platinum group metal processing value chain-a review, Metals 8 (2018) 203, https://doi.org/10.3390/met8040203.

[12] M.L. Grilli, A.E. Slobozeanu, C. Larosa, D. Paneva, I. Yakoumis, Z. Cherkezova-Zheleva, Platinum group metals: green recovery from spent auto-catalysts and reuse in new catalysts-a review, Crystals 13 (2023) 550, https://doi.org/10.3390/cryst13040550.

[13] J. Utomo, R. Kurniawan, M.S. Nuroni, A.A. Fibriyanti, A. Fuad, N. Mufti, E. Latifah, Recovery of platinum from spent removing catalyst of Pt/Al_2O_3 by ultrasonic-assisted acid leaching, in: International Conference on Condensed Matters and Advanced Materials (IC2MAM), Univ Negeri Malang, Malang, Indonesia, 2018.

[14] Z. Wiecka, M. Rzelewska-Piekut, M. Regel-Rosocka, Recovery of platinum group metals from spent automotive converters by leaching with organic and inorganic acids and extraction with quaternary phosphonium salts, Sep. Purif. Technol. 280 (2022) 119933, https://doi.org/10.1016/j.seppur.2021.119933.

[15] S.M. Sadeghi, H.M.V.M. Soares, A sustainable hydrometallurgical strategy for recycling efficiently platinum from spent reforming petroleum catalyst, Environ. Sci. Pollut. Res. 30 (2023) 101410–101423, https://doi.org/10.1007/s11356-023-28964-1.

[16] S. Sun, W. Zhao, C. Jin, W. He, G. Li, H. Zhu, Efficient HCl leaching of platinum group metals from waste three-way catalysts: a study on kinetics and mechanisms, Environ. Res. 238 (2023) 117148, https://doi.org/10.1016/j.envres.2023.117148.

[17] M.A. Barakat, M.H.H. Mahmoud, Recovery of platinum from spent catalyst, Hydrometallurgy 72 (2004) 179–184, https://doi.org/10.1016/s0304-386x(03)00141-5.

[18] M.K. Jha, J.-c. Lee, M.-s. Kim, J. Jeong, B.-S. Kim, V. Kumar, Hydrometallurgical recovery/recycling of platinum by the leaching of spent catalysts: a review, Hydrometallurgy 133 (2013) 23–32, https://doi.org/10.1016/j.hydromet.2012.11.012.

[19] M.K. Jha, D. Gupta, J.-c. Lee, V. Kumar, J. Jeong, Solvent extraction of platinum using amine based extractants in different solutions: a review, Hydrometallurgy 142 (2014) 60–69, https://doi.org/10.1016/j.hydromet.2013.11.009.

[20] H. Zheng, Y. Ding, Q. Wen, B. Liu, S. Zhang, Separation and purification of platinum group metals from aqueous solution: recent developments and industrial applications, Resour. Conserv. Recycl. 167 (2021) 105417, https://doi.org/10.1016/j.resconrec.2021.105417.

[21] G. Schreier, C. Edtmaier, Separation of Ir, Pd and Rh from secondary Pt scrap by precipitation and calcination, Hydrometallurgy 68 (2003) 69–75, https://doi.org/10.1016/s0304-386x(02)00194-9.

[22] K.-m. Liu, Y.-r. Qiu, Y. Li, Preparation of high purity platinum nitrate using spent Pt-Rh catalyst from the production of nitric acid, J. Cent. South Univ. 30 (2023) 85–94, https://doi.org/10.1007/s11771-022-5214-3.

[23] C.R.K. Rao, D.C. Trivedi, Chemical and electrochemical depositions of platinum group metals and their applications, Coord. Chem. Rev. 249 (2005) 613–631, https://doi.org/10.1016/j.ccr.2004.08.015.

[24] J.-c. Lee, H.-J. Kurniawan, K.W. Hong, S. Kim Chung, Separation of platinum, palladium and rhodium from aqueous solutions using ion exchange resin: a review, Sep. Purif. Technol. 246 (2020) 116896, https://doi.org/10.1016/j.seppur.2020.116896.

[25] H. Liu, S. Ning, S. Zhang, X. Wang, L. Chen, T. Fujita, Y. Wei, Preparation of a mesoporous ion-exchange resin for efficient separation of palladium from simulated electroplating wastewater, J. Environ. Chem. Eng. 10 (2022) 106966, https://doi.org/10.1016/j.jece.2021.106966.

[26] B. Li, W. Xiong, X. Zhou, H. Zhu, M. Li, L. Yang, P. Shao, Targeting of platinum capture under 1+1 aqua regia using robust and recyclable polymeric polyamine resin: adsorption performance and mechanism, Environ. Res. 227 (2023) 115814, https://doi.org/10.1016/j.envres.2023.115814.

[27] T. Vincent, A. Parodi, E. Guibal, Pt recovery using Cyphos IL-101 immobilized in biopolymer capsules, Sep. Purif. Technol. 62 (2008) 470–479, https://doi.org/10.1016/j.seppur.2008.02.025.

[28] O. Grad, M. Ciopec, A. Negrea, N. Duțeanu, G. Vlase, P. Negrea, C. Dumitrescu, T. Vlase, R. Vodă, Precious metals recovery from aqueous solutions using a new adsorbent material, Sci. Rep. 11 (2021) 2016, https://doi.org/10.1038/s41598-021-81680-z.

[29] M. Yamada, S. Kimura, M.R. Gandhi, A. Shibayama, Environmentally friendly Pd (II) recovery from spent automotive catalysts using resins impregnated with a pincer-type extractant, Sci. Rep. 11 (2021) 365, https://doi.org/10.1038/s41598-020-79614-2.

[30] F. Nkinahamira, A. Alsbaiee, Y.W. Wang, X.Y. Yang, T.Y. Chen, M.X. Cao, M. L. Feng, Q. Sun, C.P. Yu, Recovery and purification of rare earth elements from wastewater and sludge using a porous magnetic composite of β-cyclodextrin and silica doped with PC88A, Sep. Purif. Technol. 266 (2021) 118589, https://doi.org/10.1016/j.seppur.2021.118589.

[31] A. Wolowicz, Z. Hubicki, The use of the chelating resin of a new generation Lewatit MonoPlus TP-220 with the bis-picolylamine functional groups in the removal of selected metal ions from acidic solutions, Chem. Eng. J. 197 (2012) 493–508, https://doi.org/10.1016/j.cej.2012.05.047.

[32] M. Iwase, K. Isobe, L. Zheng, S. Takano, Y. Sohrin, Solid-phase extraction of palladium, platinum, and gold from water samples: comparison between a chelating resin and a chelating fiber with ethylenediamine groups, Anal. Sci. 39 (2023) 695–704, https://doi.org/10.1007/s44211-023-00270-3.

[33] J. Shen, Y. Dai, F. Xia, X. Zhang, Polyacrylamide/EDTA-modified chitosan/graphene oxide hydrogels as an adsorbent and supercapacitor for sustainable applications, Sustain. Mater. Technol. 36 (2023) e00586, https://doi.org/10.1016/j.susmat.2023.e00586.

[34] H. Chaudhuri, C.-R. Lim, Y.-S. Yun, Single-step synthesis of prominently selective and easily regenerable POSS functionalized with high loadings of sulfur and carboxylic acids, J. Mater. Chem. A (2023), https://doi.org/10.1039/d3ta05202h.

[35] M. Wojnicki, P. Nabec, M. Luty-Blocho, R. Socha, X. Yang, Z. Pedzich, Batch reactor vs. flow column - mechanistic investigation and modeling of Au(III) ions adsorption from aqueous solutions containing Ni^{2+}, Na^{+}, Cl^{-} and ClO_4^{-} as impurities, sustainable, Mater.Technol. 23 (2020) e00142, https://doi.org/10.1016/j.susmat.2019.e00142.

[36] S.-P. Feng, K. Huang, Enhanced separation of Pd(II) and Pt(IV) from hydrochloric acid aqueous solution using 2-((2-methoxyethyl)thio)-1H-benzimidazole, Rare Metals 39 (2020) 1473–1482, https://doi.org/10.1007/s12598-020-01545-8.

[37] R.G. Pearson, Acids and bases, Science (New York, N.Y.) 151 (1966) 172–177, https://doi.org/10.1126/science.151.3707.172.

[38] E. Nieboer, D.H.S. Richardson, The replacement of the non-descript therm heavy-metals by a biologically and chemically significant classification of metal-ions, Environ. Pollut. Ser. B 1 (1980) 3–26, https://doi.org/10.1016/0143-148x(80)90017-8.

[39] H. Chaudhuri, C.-R. Lim, Y.-S. Yun, Amino- and sulfur-containing POSS for highly efficient and selective extraction of platinum group elements from acidic solution, J. Clean. Prod. 434 (2024) 139912, https://doi.org/10.1016/j.jclepro.2023.139912.

[40] A.M. Atta, A.O. Ezzat, Y.M. Moustafa, N.I. Sabeela, A.M. Tawfeek, H.A. Al-Lohedan, A.I. Hashem, Synthesis of new magnetic crosslinked poly (ionic liquid) nanocomposites for fast Congo Red removal from industrial wastewater, Nanomaterials 9 (2019) 1286, https://doi.org/10.3390/nano9091286.

[41] O. Falyouna, O. Eljamal, I. Maamoun, A. Tahara, Y. Sugihara, Magnetic zeolite synthesis for efficient removal of cesium in a lab-scale continuous treatment system, J. Colloid Interface Sci. 571 (2020) 66–79, https://doi.org/10.1016/j.jcis.2020.03.028.

[42] X. Chen, H. Mi, C. Ji, C. Lei, Z. Fan, C. Yu, L. Sun, Hierarchically porous carbon microfibers for solid-state supercapacitors, J. Mater. Sci. 55 (2020) 5510–5521, https://doi.org/10.1007/s10853-020-04376-1.

[43] Q. Wu, Y. Xian, Z. He, Q. Zhang, J. Wu, G. Yang, X. Zhang, H. Qi, J. Ma, Y. Xiao, et al., Adsorption characteristics of Pb(II) using biochar derived from spent mushroom substrate, Sci. Rep. 9 (2019) 15999, https://doi.org/10.1038/s41598-019-52554-2.

[44] Q. Zhang, H. Chen, X. Han, J. Cai, Y. Yang, M. Liu, K. Zhang, Graphene-encapsulated nanosheet-assembled zinc–nickel–cobalt oxide microspheres for enhanced lithium storage, ChemSusChem 9 (2016) 186–196, https://doi.org/10.1002/cssc.201501151.

[45] H. Tang, W. Li, H. Jiang, R. Lin, Z. Wang, J. Wu, G. He, P.R. Shearing, D.J.L. Brett, ZIF-8-derived hollow carbon for efficient adsorption of antibiotics, Nanomaterials 9 (2019) 117, https://doi.org/10.3390/nano9010117.

[46] P. Sharma, A.P. Singh, A covalently anchored 2,4,6-triallyloxy-1,3,5-triazine Pd(II) complex over a modified surface of SBA-15: catalytic application in hydrogenation reaction, RSC Adv. 4 (2014) 58467–58475, https://doi.org/10.1039/C4RA10002F.

[47] S. Madani, N. Charef, A. Hellal, D.L. Garcia, M.F. Garcia, L. Arrar, M.S. Mubarak, Synthesis, density functional theory studies, and sorption properties toward some divalent heavy metal ions of a new polystyrene-supported 4-(5-mercapto-1,3,4-thiadiazol-2-ylimino) pentan-2-one polymer, J. Appl. Polym. Sci. 137 (2020) 48289, https://doi.org/10.1002/app.48289.

[48] R.K. Dani, M.K. Bharty, O. Prakash, R.K. Singh, B. Prashanth, S. Singh, N.K. Singh, Ni(II) and co(III) complexes of 5-methyl-1,3,4-thiadiazole-2-thiol: syntheses, spectral, structural, thermal analysis, and DFT calculation, J. Coord. Chem. 68 (2015) 2666–2681, https://doi.org/10.1080/00958972.2015.1057131.

[49] C.E. Dogan, G. Akcin, Sorption and desorption of lead on 5-amino-1,3,4-thiadiazole-2-thiol immobilized silica gel by flame atomic absorption spectrometry (FAAS), Instrum. Sci. Technol. 36 (2008) 476–492, https://doi.org/10.1080/10739140802234907.

[50] J.K. Bediako, S.W. Park, J.-W. Choi, M.-H. Song, Y.-S. Yun, High-performance and acid-tolerant polyethylenimine-aminated polyvinyl chloride fibers: fabrication and application for recovery of platinum from acidic wastewaters, J. Environ. Chem. Eng. 7 (2019) 102839, https://doi.org/10.1016/j.jece.2018.102839.

[51] X. Zhang, Y. Yang, Y. Wu, X. Xu, Z. Huang, Exploring imidazolium-based poly(ionic liquids) as adsorbents for Pt(IV) removal: the impact of N3 substituents, J. Environ. Chem. Eng. 11 (2023) 110683, https://doi.org/10.1016/j.jece.2023.110683.

[52] A.J. Bard, L.R. Faulkner, Electrochemical Methods: Fundamentals and Applications, 2nd ed., J. Wiley & Sons, Ltd., New York, N.Y. (USA), 2000.

[53] T. Mang, B. Breitscheidel, P. Polanek, H. Knözinger, Adsorption of platinum complexes on silica and alumina: preparation of non-uniform metal distributions within support pellets, Appl. Catal., A 106 (1993) 239–258, https://doi.org/10.1016/0926-860X(93)80180-X.

[54] W.A. Spieker, J. Liu, J.T. Miller, A.J. Kropf, J.R. Regalbuto, An EXAFS study of the co-ordination chemistry of hydrogen hexachloroplatinate(IV): 1. Speciation in aqueous solution, Appl. Catal., A 232 (2002) 219–235, https://doi.org/10.1016/S0926-860X(02)00116-3.

[55] M. Iglesias, E. Anticó, V. Salvadó, Characterization of metalfix-chelamine and its application in precious metal adsorption, Solvent Extr. Ion Exch. 18 (2000) 965–979, https://doi.org/10.1080/07366290008934717.

[56] R. Dobrowolski, M. Oszust-Cieniuch, J. Dobrzyńska, M. Barczak, Amino-functionalized SBA-15 mesoporous silicas as sorbents of platinum (IV) ions, Colloids Surf. A Physicochem. Eng. Asp. 435 (2013) 63–70, https://doi.org/10.1016/j.colsurfa.2012.12.001.

[57] V. Neagu, C. Paduraru, I. Bunia, L. Tofan, Platinum (IV) recovery from chloride solution by functionalized acrylic copolymers, J. Environ. Manag. 91 (2009) 270–276, https://doi.org/10.1016/j.jenvman.2009.08.013.

[58] D. Parajuli, K. Khunathai, C.R. Adhikari, K. Inoue, K. Ohto, H. Kawakita, M. Funaoka, K. Hirota, Total recovery of gold, palladium, and platinum using lignophenol derivative, Miner. Eng. 22 (2009) 1173–1178, https://doi.org/10.1016/j.mineng.2009.06.003.

[59] L.M.K. Alifkhanova, K.Y. Lopunova, A.A. Marchuk, Y.S. Petrova, A.V. Pestov, L. K. Neudachina, Features of sorption preconcentration of noble metal ions with sulfoethylated amino polymers, Russ. J. Inorg. Chem. 66 (2021) 909–915, https://doi.org/10.1134/s0036023621060024.

[60] H. Chaudhuri, X.Y. Lin, Y.S. Yun, Graphene oxide-based dendritic adsorbent for the excellent capturing of platinum group elements, J. Hazard. Mater. 451 (2023) 131206, https://doi.org/10.1016/j.jhazmat.2023.131206.

[61] X. Feng, Y. He, Z. Xing, M. Zhang, R. Li, G. Wu, Highly selective adsorption of Pt (IV) from spent catalyst by polyethyleneimine functionalized polyethylene/polypropylene non-woven fabric, J. Appl. Polym. Sci. 140 (2023) 53322, https://doi.org/10.1002/app.53322.

[62] P. Ramakul, Y. Yanachawakul, N. Leepipatpiboon, N. Sunsandee, Biosorption of palladium(II) and platinum(IV) from aqueous solution using tannin from Indian almond (*Terminalia catappa* L.) leaf biomass: kinetic and equilibrium studies, Chem. Eng. J. 193 (2012) 102–111, https://doi.org/10.1016/j.cej.2012.04.035.

[63] D. Xue, T. Li, Y. Liu, Y. Yang, Y. Zhang, J. Cui, D. Guo, Selective adsorption and recovery of precious metal ions from water and metallurgical slag by polymer brush graphene-polyurethane composite, React. Funct. Polym. 136 (2019) 138–152, https://doi.org/10.1016/j.reactfunctpolym.2018.12.026.

[64] D.H.K. Reddy, W. Wei, L. Shuo, M.-H. Song, Y.-S. Yun, Fabrication of stable and regenerable amine functionalized magnetic nanoparticles as a potential material for Pt(IV) recovery from acidic solutions, ACS Appl. Mater. Interfaces 9 (2017) 18650–18659, https://doi.org/10.1021/acsami.6b16813.

[65] Y. Marcus, Ion Properties, Marcel Dekker, Inc., New York, NY, 1997, 259 pp.

[66] H.N. Tran, E.C. Lima, R.-S. Juang, J.-C. Bollinger, H.-P. Chao, Thermodynamic parameters of liquid-phase adsorption process calculated from different equilibrium constants related to adsorption isotherms: a comparison study, J. Environ. Chem. Eng. 9 (2021) 106674, https://doi.org/10.1016/j.jece.2021.106674.

[67] A. Melchior, S.G. Lanas, M. Valiente, M. Tolazzi, Thermodynamics of sorption of platinum on superparamagnetic nanoparticles functionalized with mercapto groups, J. Therm. Anal. Calorim. 134 (2018) 1261–1266, https://doi.org/10.1007/s10973-018-7408-3.

[68] N. Rahman, I. Ahmad, Insights into the statistical physics modeling and fractal like kinetic approach for the adsorption of As(III) on coordination polymer gel based on zirconium(IV) and 2-thiobarbituric acid, J. Hazard. Mater. 457 (2023) 131783, https://doi.org/10.1016/j.jhazmat.2023.131783.

[69] Y.T. Yang, X.Z. Wei, J.M. Wan, Z.F. Meng, Equilibrium and kinetic characteristic of adsorption of Cu^{2+}, Pb^{2+} on a novel anionic starch microspheres, Water Air Soil Pollut. 219 (2011) 103–112, https://doi.org/10.1007/s11270-010-0690-8.

[70] T. Saeed, A. Naeem, I.U. Din, M. Farooq, I.W. Khan, M. Hamayun, T. Malik, Synthesis of chitosan composite of metal-organic framework for the adsorption of dyes; kinetic and thermodynamic approach, J. Hazard. Mater. 427 (2022) 127902, https://doi.org/10.1016/j.jhazmat.2021.127902.

[71] V.C. Srivastava, I.D. Mall, I.M. Mishra, Adsorption thermodynamics and isosteric heat of adsorption of toxic metal ions onto bagasse fly ash (BFA) and rice husk ash (RHA), Chem. Eng. J. 132 (2007) 267–278, https://doi.org/10.1016/j.cej.2007.01.007.

[72] A.B. Wassie, V.C. Srivastava, Chemical treatment of teff straw by sodium hydroxide, phosphoric acid and zinc chloride: adsorptive removal of chromium, Int. J. Environ. Sci. Technol. 13 (2016) 2415–2426, https://doi.org/10.1007/s13762-016-1080-6.

[73] M.H. Morcali, B. Zeytuncu, S. Akman, O. Yucel, Preparation and sorption behavior of DEAE-cellulose-thiourea-glutaraldehyde sorbent for Pt(IV) and Pd(II) from leaching solutions, Desalin. Water Treat. 57 (2016) 6582–6593, https://doi.org/10.1080/19443994.2015.1010591.

[74] O.E. Fayemi, A.S. Ogunlaja, P.F.M. Kempgens, E. Antunes, N. Torto, T. Nyokong, Z. R. Tshentu, Adsorption and separation of platinum and palladium by polyamine functionalized polystyrene-based beads and nanofibers, Miner. Eng. 53 (2013) 256–265, https://doi.org/10.1016/j.mineng.2013.06.006.

[75] A.N. Nikoloski, K.-L. Ang, D. Li, Recovery of platinum, palladium and rhodium from acidic chloride leach solution using ion exchange resins, Hydrometallurgy 152 (2015) 20–32, https://doi.org/10.1016/j.hydromet.2014.12.006.

[76] P.P. Sun, T.Y. Kim, B.J. Min, H.I. Song, S.Y. Cho, Recovery of platinum from chloride leaching solutions of spent reforming catalysts by ion exchange, Mater. Trans. 56 (2015) 738–742, https://doi.org/10.2320/matertrans.M2015027.

[77] M.-H. Song, S. Kim, D.H.K. Reddy, W. Wei, J.K. Bediako, S. Park, Y.-S. Yun, Development of polyethyleneimine-loaded core-shell chitosan hollow beads and their application for platinum recovery in sequential metal scavenging fill-and-draw process, J. Hazard. Mater. 324 (2017) 724–731, https://doi.org/10.1016/j.jhazmat.2016.11.047.

[78] R. Tovar-Gómez, M.d.R. Moreno-Virgen, J. Moreno-Pérez, A. Bonilla-Petriciolet, V. Hernández-Montoya, C.J. Durán-Valle, Analysis of synergistic and antagonistic adsorption of heavy metals and acid blue 25 on activated carbon from ternary systems, Chem. Eng. Res. Des. 93 (2015) 755–772, https://doi.org/10.1016/j.cherd.2014.07.012.

[79] K. Li, M. Li, D. Xue, Solution-phase electronegativity scale: insight into the chemical behaviors of metal ions in solution, J. Phys. Chem. A 116 (2012) 4192–4198, https://doi.org/10.1021/jp300603f.

[80] D.A. Yatsenko, V.P. Pakharukova, S.V. Tsybulya, Low temperature transitional aluminas: structure specifics and related X-ray diffraction features, Crystals 11 (2021) 690, https://doi.org/10.3390/cryst11060690.

[81] M.S. Al-Iessa, B.Y. Al-Zaidi, R.S. Almukhtar, Z.M. Shakor, I. Hamawand, Optimization of polypropylene waste recycling products as alternative fuels through non-catalytic thermal and catalytic hydrocracking using fresh and spent Pt/Al_2O_3 and $NiMo/Al_2O_3$ catalysts, Energies 16 (2023) 4871, https://doi.org/10.3390/en16134871.

[82] A.D.V. Souza, C.C. Arruda, L. Fernandes, M.L.P. Antunes, P.K. Kiyohara, R. Salomão, Characterization of aluminum hydroxide ($Al(OH)_3$) for use as a porogenic agent in castable ceramics, J. Eur. Ceram. Soc. 35 (2015) 803–812, https://doi.org/10.1016/j.jeurceramsoc.2014.09.010.

[83] M.E. Silva Júnior, M.O. Palm, D.A. Duarte, R.C. Catapan, Catalytic Pt/Al_2O_3 monolithic foam for ethanol reforming fabricated by the competitive impregnation method, ACS Omega 8 (2023) 6507–6514, https://doi.org/10.1021/acsomega.2c06870.

[84] T. Suoranta, O. Zugazua, M. Niemelä, P. Perämäki, Recovery of palladium, platinum, rhodium and ruthenium from catalyst materials using microwave-assisted leaching and cloud point extraction, Hydrometallurgy 154 (2015) 56–62, https://doi.org/10.1016/j.hydromet.2015.03.014.

[85] H. Zheng, Y. Ding, Q. Wen, S. Zhao, X. He, S. Zhang, C. Dong, Slag design and iron capture mechanism for recovering low-grade Pt, Pd, and Rh from leaching residue of spent auto-exhaust catalysts, Sci. Total Environ. 802 (2022) 149830, https://doi.org/10.1016/j.scitotenv.2021.149830.

[86] H. Dong, J. Zhao, W. Tong, H. Cui, Y. Wu, Concentrating Pt from a spent alumina carrier catalyst by a roast-leach process, Metall. Res. Technol. 116 (2019) 204, https://doi.org/10.1051/metal/2018115.

[87] E. Prasetyo, C. Anderson, Platinum group elements recovery from used catalytic converters by acidic fusion and leaching, Metals 10 (2020) 485, https://doi.org/10.3390/met10040485.

[88] J.d.O. Demarco, J.S. Cadore, H.M. Veit, H.B. Madalosso, E.H. Tanabe, D.A. Bertuol, Leaching of platinum group metals from spent automotive catalysts using organic acids, Miner. Eng. 159 (2020) 106634, https://doi.org/10.1016/j.mineng.2020.106634.

[89] M. Yamada, M.R. Gandhi, U.M.R. Kunda, T. Mori, K. Haga, A. Shibayama, Recovery of Pd(II) from leach solutions of automotive catalysts by solvent extraction with new thiophosphate extractants, Hydrometallurgy 191 (2020) 105221, https://doi.org/10.1016/j.hydromet.2019.105221.

[90] R. Kurniawan, M.S. Nuroni, A.A. Fibriyanti, J. Utomo, A. Fuad, N. Mufti, E. Latifah, Time-dependent ultrasonic assisted recovery of platinum from spent removing catalyst of Pt/Al_2O_3 by acid leaching, in: International Conference on Condensed Matters and Advanced Materials (IC2MAM), Univ Negeri Malang, Malang, Indonesia, 2018, https://doi.org/10.011088/011757-012899x/012515/012061/012068, 012068.